Quantifying lithological variability in the mantle

Oliver Shorttle [a,*], John Maclennan [a], Sarah Lambart [b]

[a] *Department of Earth Sciences, University of Cambridge, Downing Street, Cambridge CB2 3EQ, UK*
[b] *Division of Geological and Planetary Sciences, California Institute of Technology, Pasadena, CA 91125, USA*

ABSTRACT

We present a method that can be used to estimate the amount of recycled material present in the source region of mid-ocean ridge basalts by combining three key constraints: (1) the melting behaviour of the lithologies identified to be present in a mantle source, (2) the overall volume of melt production, and (3) the proportion of melt production attributable to melting of each lithology. These constraints are unified in a three-lithology melting model containing lherzolite, pyroxenite and harzburgite, representative products of mantle differentiation, to quantify their abundance in igneous source regions.

As a case study we apply this method to Iceland, a location with sufficient geochemical and geophysical data to meet the required observational constraints. We find that to generate the 20 km of igneous crustal thickness at Iceland's coasts, with $30 \pm 10\%$ of the crust produced from melting a pyroxenitic lithology, requires an excess mantle potential temperature (ΔTp) of $\geqslant 130\,^\circ C$ (Tp $\geqslant 1460\,^\circ C$) and a source consisting of at least 5% recycled basalt. Therefore, the mantle beneath Iceland requires a significant excess temperature to match geophysical and geochemical observations: lithological variation alone cannot account for the high crustal thickness. Determining a unique source solution is only possible if mantle potential temperature is known precisely and independently, otherwise a family of possible lithology mixtures is obtained across the range of viable ΔTp. For Iceland this uncertainty in ΔTp means that the mantle could be >20% harzburgitic if $\Delta Tp > 150\,^\circ C$ (Tp > $1480\,^\circ C$).

The consequences of lithological heterogeneity for plume dynamics in various geological contexts are also explored through thermodynamic modelling of the densities of lherzolite, basalt, and harzburgite mixtures in the mantle. All lithology solutions for Iceland are buoyant in the shallow mantle at the ΔTp for which they are valid, however only lithology mixtures incorporating a significant harzburgite component are able to reproduce recent estimates of the Iceland plume's volume flux. Using the literature estimates of the amount of recycled basalt in the sources of Hawaiian and Siberian volcanism, we found that they are negatively buoyant in the upper mantle, even at the extremes of their expected ΔTp. One solution to this problem is that low density refractory harzburgite is a more ubiquitous component in mantle plumes than previously acknowledged.

1. Introduction

Plate tectonic motions have been cycling material from the Earth's surface into the deep mantle for several billion years, connecting the development of the atmosphere and oceans to the generation of chemical heterogeneity in the Earth's interior. The marble-cake mantle that we find today preserves a record of planetary differentiation (Allègre and Turcotte, 1986), which provides information about conditions early in Earth's history, and on the mantle dynamics driving planetary evolution.

The difficulty of sampling material from the Earth's deep interior poses a major obstacle to understanding its current and past states. One means of accessing this information is by studying the volcanic products erupted at mid-ocean ridges (MOR), arcs and intra-plate settings. Of these, MOR basalts (MORB) provide our best chance of obtaining information on the thermo-chemical state of the convecting upper mantle for a number of reasons. Firstly, there is only a thin layer of young igneous crust between source and surface, minimising the possibility of contamination from old radiogenic continental crust and lithosphere. Secondly, if MOR act as passive linear samplers of the upper mantle, then the compositional distribution of the material rising under MOR is the same as the global distribution of compositions in the uppermost convecting mantle. Thirdly, the coverage of the globe by MOR allows us to investigate global spatial patterns of mantle chemistry.

* Corresponding author.
 E-mail addresses: os258@cam.ac.uk (O. Shorttle), jcm1004@cam.ac.uk (J. Maclennan), saral@ldeo.columbia.edu (S. Lambart).

In order to understand the origin and dynamics of the mantle it is necessary to have knowledge of its composition. Although the long-held lherzolite model explains many features of mantle structure (Ringwood, 1962), a predicted ∼10% of basaltic crust will have been returned to the mantle over Earth's history (Hofmann, 1997; Stracke et al., 1999). Given that basalts form by the depletion of some primary lherzolitic lithology, a large return flux of basalt to the Earth's interior necessitates a highly lithologically heterogeneous mantle, containing refractory harzburgitic and fusible pyroxenitic/eclogitic domains with a complete spectrum of lithologies of intermediate fertility in between. However, including such a wealth of mantle diversity in a melting model is currently beyond our ability, and in any case would be unconstrained by geochemical observations in most settings. Therefore, we reduce the spectrum of mantle lithological variability to a consideration of three representative lithologies, which between them encompass most of the expected range from recycling: (1) an aluminous lherzolite, representing depleted upper mantle and presumably the most abundant lithology in MORB genesis; (2) a pyroxenite, representing recycled basalt and an example of a high-productivity lithology; (3) a harzburgite, to represent the refractory residues left after melt extraction, which will have low productivity during any further melting. We develop a method that can be used to quantify the abundance of these three lithologies in basalt source regions.

1.1. Previous estimates of the lithological character of the mantle

Recycled oceanic crust was first invoked as a mantle component to explain the high trace element concentrations and radiogenic isotopic compositions of ocean island volcanics (Chase, 1981; Hofmann and White, 1982). Following the 'marble-cake' mantle model of Allègre and Turcotte (1986), Prinzhofer et al. (1989) explored the role of a mixed peridotite–pyroxenite source in generating the local variation in trace element and isotopic compositions of basalts from the East Pacific Rise. Hirschmann and Stolper (1996) extended this logic to MORB globally, suggesting a mixed lherzolite–garnet pyroxenite source as the cause of the signature of garnet in MORB. The crucial methodological insight of Hirschmann and Stolper (1996) was to couple the geochemical constraints with a requirement to match typical MOR crustal thickness (∼7 km, White et al., 1992), combining these chemical and physical observations with a model of mantle melting. This model allowed for the higher productivity of pyroxenite compared with lherzolite lithologies to be accounted for when estimating the abundance of source pyroxenite. With these observational and model constraints, Hirschmann and Stolper (1996) estimated that 5% of MORB mantle-source could be formed of pyroxenite.

A number of authors have recently attempted to estimate the proportion of pyroxenite in various settings using olivine compositions or the trace and major element compositions of basalts (e.g., Sobolev et al., 2005, 2007, 2008; Lambart et al., 2009; Pietruszka et al., 2013). By combining Os isotopes and olivine compositions, Sobolev et al. (2008) concluded that ∼40% of the mass of some Icelandic melts were derived from pyroxenite melting. However, this estimation does not formally include the requirement to match melt volumes with source composition, nor do the authors perform an investigation into how productivity differences affect the estimates of source lithology. Shorttle and Maclennan (2011) identified lithological heterogeneity beneath Iceland using basalt major element compositions and produced a melting model to explore pyroxenite's effect on melt production. However, they did not use geochemical constraints to define the fraction of melt production derived from pyroxenite melting, nor did they rigorously constrain source composition.

A separate issue overlooked by the above methods is the role and abundance of refractory material in the mantle. The unradiogenic Pb isotopic compositions found in North Atlantic basalts associated with the Iceland plume, and their offset from depleted MORB mantle values, led Thirlwall (1995) and Kerr et al. (1995) to infer the presence of refractory domains in plume sources. Subsequent to these studies Fitton et al. (1997) used the Nb–Zr–Y trace element systematics of Icelandic basalts to identify a distinct depleted endmember for the Iceland plume. Nd and Hf isotope systems have been used to validated this result for Icelandic basalts (Kempton et al., 2000; Fitton et al., 2003), and also compiled from MORB globally to highlight the importance of depleted domains (Salters et al., 2011). Abyssal peridotites provide an independent line of evidence for the presence of highly depleted domains in the mantle. Stracke et al. (2011) showed that clinopyroxenes from Gakkel Ridge abyssal peridotites contain extremely radiogenic Nd and Hf isotopic compositions, extending beyond the values observed in MORB. Importantly for the issue of melt generation and mantle dynamics, Stracke et al. (2011) also found that the Hf isotopes correlated with major and trace element indices of depletion, meaning these domains with radiogenic Hf are also refractory. These results suggest that refractory domains could be a ubiquitous upper mantle component. However, identifying the role of refractory domains in basalt genesis remains challenging and we are lacking in tools to quantify the combined effect of refractory and fusible heterogeneity on melt production.

As the earlier Hirschmann and Stolper (1996) analysis showed, neither geochemical nor geophysical constraints alone are sufficient to quantify mantle lithological variability. The abundant observational evidence for both depleted and enriched mantle domains, forces us to develop a method to formally quantify the involvement of both of these sources in the melting process, even if the refractory domain contributes little melt. Here we demonstrate how geochemical and geophysical observations can be combined with a model of three lithology melting to quantify the thermochemical state of the mantle.

1.2. Approach

This contribution is split into three sections, each exploring constraints on source lithology.

Section 2 contains a description of a method for estimating the mass fraction of pyroxenite derived melts forming the average Icelandic crust (F_{px}^{melt}). Using the geochemistry of Icelandic basalts we form a mass budget of enriched and depleted melts and find that $F_{px}^{melt} = 0.3 \pm 0.1$.

In Section 3 we project the calculated value of F_{px}^{melt} back into a mass fraction of solid mantle material. We develop a melting model that includes lherzolite, pyroxenite and harzburgite lithologies to resolve the influence of their different productivities on F_{px}^{melt}. Coupling observational constraints on F_{px}^{melt} and melt production allows a single source lithology mixture to be identified. However, the abundance of lherzolite and harzburgite lithologies in the source is strongly dependent on having knowledge of mantle potential temperature (Tp).

We next investigate the dynamical implications of lithological heterogeneity as a possible additional constraint on source. In Section 4 we model the densities of lherzolite–pyroxenite–harzburgite mixtures to assess their buoyancy in the upper mantle and consequences for plume volume flux. All our valid source solutions for Iceland are buoyant. However, we show that some previous literature estimates for Hawaiian and Siberian trap volcanism, which involve >15% pyroxenite in the source, are not likely to be buoyant even in mantle plumes with large ΔTp.
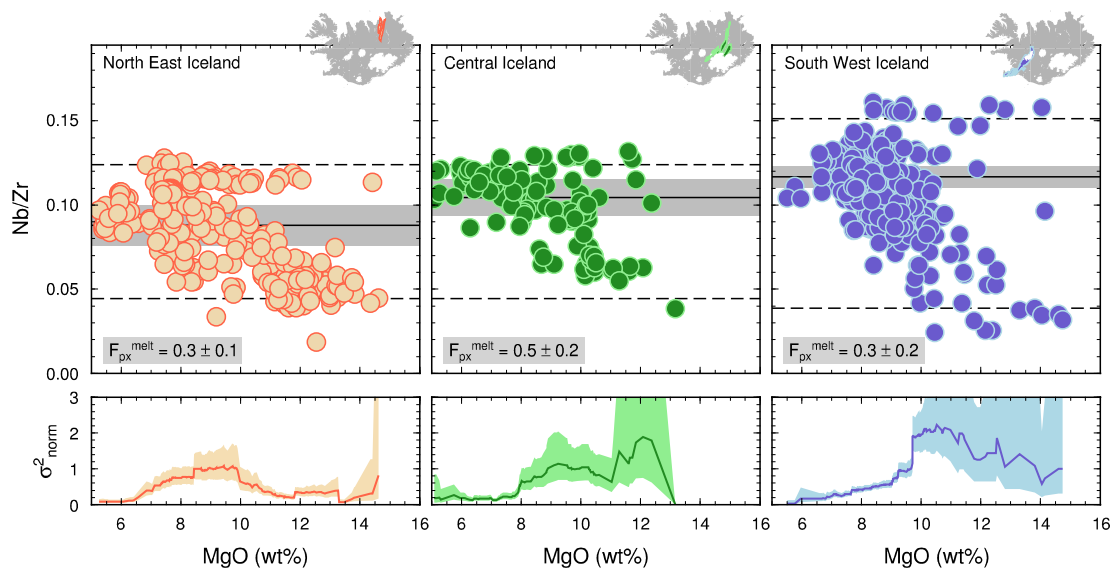
Fig. 1. The geochemical variability recorded in Icelandic whole-rock samples. The top three panels show how in lavas from each zone Nb/Zr evolves as MgO drops. Solid horizontal lines mark the volume average composition ($\overline{Nb}/\overline{Zr}$) calculated from all samples in the zone, with 1 s.e. drawn as a grey bar (see text for details). Dashed horizontal lines record the endmember Nb/Zr calculated from the highest and lowest 10% of samples from each zonal dataset (5% for south west Iceland, because of its smaller number of samples at enriched and depleted extremes) falling within a 9.5–12 wt% MgO interval (Shorttle and Maclennan, 2011). F_{px}^{melt} is calculated using Eq. (4), which mass balances the endmember compositions with the volume average crustal composition shown in each panel, uncertainty on F_{px}^{melt} is propagated from the standard deviation of the endmember compositions and mean crustal composition and quoted at 1σ. Inset maps highlight the geographic location of each volcanic system the samples are from. The bottom panels show the running normalised variance for the data in the plots above, binned in 1.5 wt% MgO intervals with a 95% confidence envelope. Data sources can be found in Appendix F.

2. Proportion of pyroxenite supplied melt

Shorttle and Maclennan (2011) established the need for lithological heterogeneity in the Icelandic mantle from the observation that the high FeO and low CaO of certain Icelandic basalts could not be reproduced by melting of a depleted lherzolite. Instead, these major element characteristics require melting of a refertilised lherzolite containing up to 50% basalt material (e.g. the pyroxenitic KG1 lithology of Kogiso et al., 1998). High FeO and low CaO in Icelandic basalts correlates with high incompatible trace element and radiogenic Sr and Pb isotopic compositions, linking typical indices of enrichment to a specific mantle lithology (Appendix A and Shorttle and Maclennan, 2011). These incompatible trace element and isotopic characteristics are a useful tracer of a magma's source history, as they have simple systematics in response to fractional crystallisation and magma mixing. In this section we use the incompatible trace element ratios of basalts to determine the aggregate melt composition and from this form a mass balance between melts from lherzolite and pyroxenite lithologies.

2.1. Calculating an aggregate melt composition

An erupted basalt is formed by a stochastic mixing and crystallisation process, with its final composition a combination of pyroxenite and lherzolite derived melts according to its melt mixing history during transport through mantle and crust (Rudge et al., 2013). The variable mixing history of basalts from single melt regions is advantageous, as it means that lithological and compositional variability is resolvable (Maclennan, 2008b; Shorttle and Maclennan, 2011). However, a corollary of this finding is that any single basalt will give a biased representation of the composition of melts being supplied from the mantle, especially at high MgO, where residence in the crust has yet to mix out primary compositional variability (Maclennan, 2008a). To remove this bias and start to reconstruct the chemical properties of the bulk mantle, we need to consider the aggregate composition of melts

being produced and the endmember melt compositions from each lithology.

In the case of Iceland, where melting is occurring at a ridge axis, the aggregate product of mantle melting is the column of new igneous crust. During a basalt's evolution in the crust it will mix with existing melt reservoirs, which on average will be more evolved and have undergone greater mixing the shallower they are in the system. These processes homogenise a diversity of mantle supplied melts, which for conservative tracers like radiogenic isotopes and incompatible trace element ratios (see Appendix B), will result in a convergence of melt compositions at low MgO towards that of the average crust (Maclennan, 2008a). The consequences of crustal mixing and fractionation processes can be seen in Fig. 1. Data from each zone displays a spread in Nb/Zr at high MgO, collapsing to a limited range by 5–6 wt% MgO. The lower panels in Fig. 1 quantify this drop in geochemical variance for each zone. The concurrent mixing and crystallisation of basalts means that by <6 wt% MgO they provide a good estimate of the average composition of mantle melts for a conservative tracer like Nb/Zr.

A test of whether the diminishing range of basalt compositions at low MgO reliably estimates the average crustal composition is to compare low MgO compositions with a direct average of all sampled basalts. We form this average by using the known volume of eruptions to calculate a volume weighted average of all the chemical data available. A volume average is formed by assigning each sample a fractional volume,

$$v_k = V_k / n_k, \qquad (1)$$

where V_k is the total erupted volume of eruption k and n_k the number of samples from that eruption. From this, the mean concentration of an element i can be calculated, appropriately weighted by each volume,

$$\bar{C}_i = \frac{\sum_{k=1}^{N_e} \sum_{x=1}^{n_k} v_k C_{xi}}{\sum_{k=1}^{N_e} V_k}, \qquad (2)$$
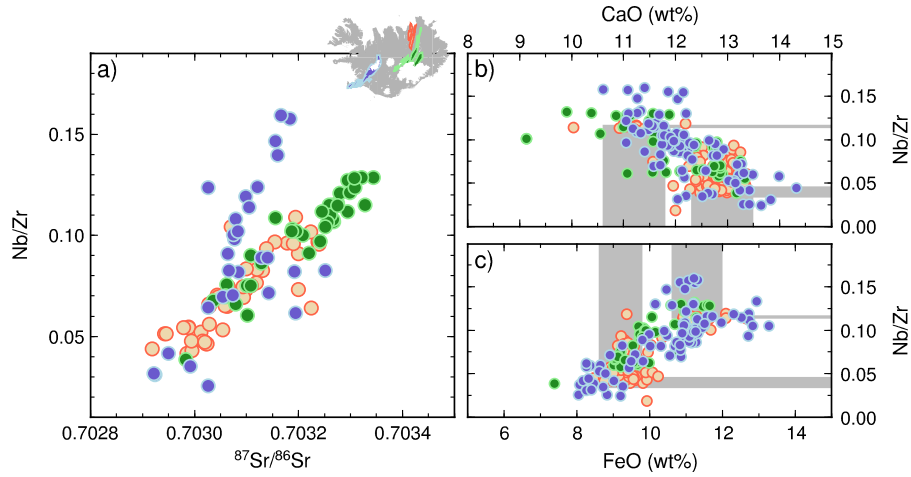
Fig. 2. (a) The relationship between the Nb/Zr of high MgO basalts (9.5–12.5 wt% MgO) and their Sr isotopic composition. The plotted data are from the subset of samples in Fig. 1 that also have Sr isotope analyses. Panels (b) and (c) show the correlation between Nb/Zr and the major element oxides, CaO in (b), and FeO in (c). Grey bars map the selection of the 10% of basalts with either the highest or lowest Nb/Zr from north east Iceland onto their corresponding major element compositions. These basalts were used by Shorttle and Maclennan (2011) to define the major element characteristics of endmember enriched and depleted Icelandic basalts, and relate them to source lithological heterogeneity. The width of the grey bars is equal to one standard deviation either side of the mean of the 10% of basalts used in defining the endmember compositions. Only basalts with MgO between 9.5 and 12.5 wt% MgO are used. Data sources in Appendix F.

where N_e is the number of eruptions. In the mixing calculation to determine the mass fraction of pyroxenite supplied melt in the crust, we are going to mass balance the incompatible trace element concentrations of endmember melts with the trace element ratio of the mean crust for the ith and jth elements. In this case the relevant mean crustal composition is

$$R_{ij} = \bar{C}_i / \bar{C}_j. \tag{3}$$

The solid horizontal black lines in Fig. 1 allow for comparison of $R_{\mathrm{Nb,Zr}}$ from Eqs. (1)–(3) with the raw data. In each case, the calculated crustal average is close to the erupted basalt compositions at low MgO.

2.2. Defining endmember melt compositions

To form the mass balance with the average crustal composition, endmember melt compositions need to be selected. Endmembers are defined by selecting the 10% of samples (5% for south west Iceland) with the highest (enriched) and lowest (depleted) Nb/Zr with MgO concentrations from 9.5 to 12 wt%. This is the same range of basalts used by Shorttle and Maclennan (2011) to characterise the major element composition of enriched and depleted Icelandic melts, and relate this major element variability to specific lithological heterogeneity in the Icelandic mantle. The estimates of the endmember melts for Nb/Zr are plotted as the black dashed horizontal lines in Fig. 1.

Implicit in our approach for characterising endmember melts and relating them to mantle lithological heterogeneity is that the trace element variation in basalt chemistry correlates with differences in mantle source. The validity of this assumption has been discussed in Shorttle and Maclennan (2011) and is further demonstrated by, (1) the isotope–Nb/Zr correlations in Fig. 2a, which show that trace element ratios are a consistent proxy for source, and (2) basalts with extremes in Nb/Zr also having extremes in most of the major elements (Figs. 2b, 2c and Appendix A). A key result from Shorttle and Maclennan (2011) for understanding our method here, is that the basalts with the extreme major element chemistries can be produced by melting of single enriched or depleted lithologies without any subsequent melt mixing/reaction. So in mass balancing between endmembers defined using trace elements, we are assuming that this directly relates to balancing the proportions of melts derived from each lithology. As our

understanding of compositional modification during melt transport develops, the major element characteristics used by Shorttle and Maclennan (2011) will have to be refined, and the ability of melts from single lithologies to produce the enriched and depleted Icelandic endmembers re-assessed. We do however, perform melting calculations using both the enriched lithology identified by Shorttle and Maclennan (2011) and an even more fusible lithology (the G2 lithology of Pertermann and Hirschmann, 2003) to evaluate the possible effect of different fusible-enriched lithologies on our estimates of the source lithology mixture.

A second important observation of Shorttle and Maclennan (2011) is that the endmember basalts from both south west and north east Iceland, despite having differences in their Nb/Zr ratios, have the same major element characteristics. This means the range of melt compositions in both areas is consistent with melting of the same two lithologies: a KLB-1 type lherzolite for the depleted basalts and a KG1 or KG2 type lithology producing the most enriched basalts. The slight trace element differences between endmember basalts in south west and north east Iceland do not create resolvable differences in their major element chemistry, which is also consistent with Nd and Sr isotopes, the extreme values of which are similar between basalts from each zone (Fig. 2a). The inter-zonal differences we see between the endmember Nb/Zr in Fig. 1 could therefore be due to slight changes in melting conditions to which the major elements are not sensitive. Spatial variation in Pb isotopes however argues for some source differences between the north and south of Iceland (Shorttle et al., 2013). Because of the potential control of melting on the trace element expression of the endmembers, we allow them to be defined on a zone by zone basis, rather than using a fixed set of endmembers for all calculations.

2.3. Calculating F_{px}^{melt}

Given the endmember trace element ratios, r_{ij}^d and r_{ij}^e, and concentrations, C_j^d and C_j^e, for depleted and enriched endmembers (superscript d and e respectively) and the average crustal composition, R_{ij}, it is now possible to form a mass balance to solve for the mass fraction of enriched melts contributing to the average crust,

$$\left[F_{px}^{melt}\right]_{ij} = \frac{r_{ij}^d - R_{ij}}{(C_j^e / C_j^d)(R_{ij} - r_{ij}^e) + (r_{ij}^d - R_{ij})}. \tag{4}$$
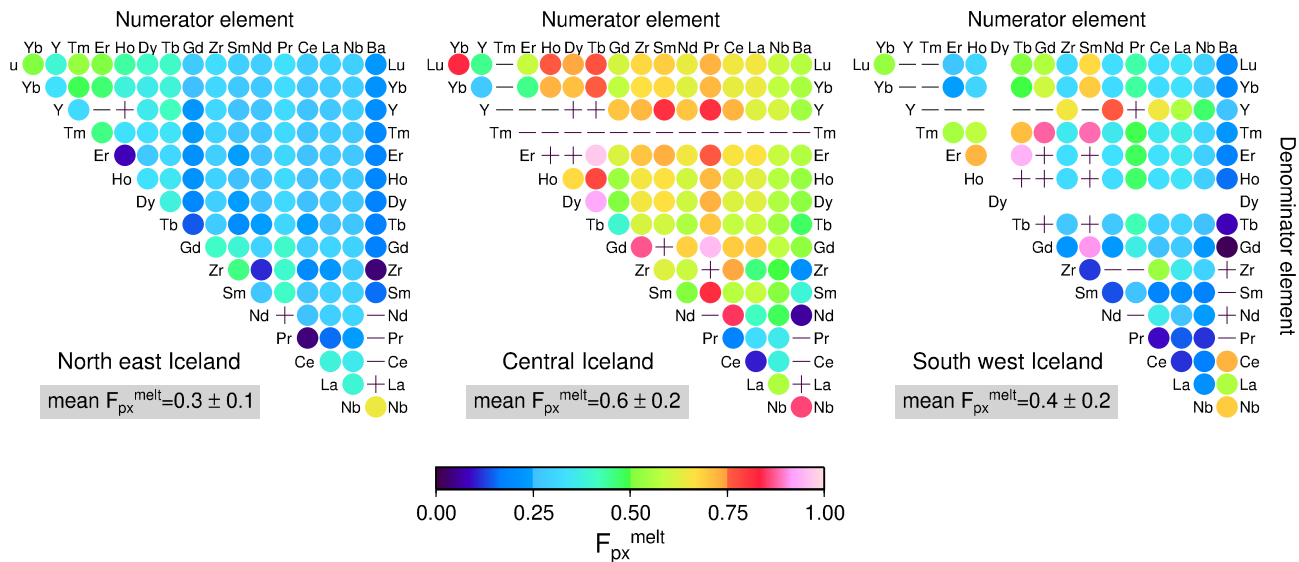
Fig. 3. Solutions of F_{px}^{melt} for a range of trace element pairs for three of Iceland's volcanic zones. F_{px}^{melt} is calculated applying the same methodology as in Fig. 1, but with different trace element pairs: for example the numerator element (Nb in Fig. 1) appears along the top axis and the denominator element (Zr from Fig. 1) along the vertical axis. The results of mass balancing between the endmember compositions and average crust using Eq. (4) to calculate F_{px}^{melt} are presented as a matrix, with each point coloured according to the F_{px}^{melt} calculated. A mean F_{px}^{melt} is found for each zone by taking the average of the matrix of results and is quoted with a 1σ uncertainty, representing the variability of the multiple F_{px}^{melt} determinations. Trace element pairs resulting in an $F_{px}^{melt} < 0$ or >1 are indicated by a '−' and '+' symbol respectively, these are left out of the average and standard deviation calculations.

The results of applying this mass balance for Nb/Zr are shown in Fig. 1: crust in north and south Iceland is made from $30 \pm 10\%$ enriched melts, whilst the higher mean Nb/Zr of basalts from central Iceland compared with north Iceland (along with central Iceland's same endmember Nb/Zr as the north) means that central Iceland's average crustal composition is balanced by $50 \pm 20\%$ of enriched melts. Uncertainty for each of these estimates of F_{px}^{melt} is propagated from the variation in endmember compositions and mean crustal composition and quoted as 1σ.

Calculations of F_{px}^{melt} are not limited to using Nb/Zr and we can use any trace element pair in Eqs. (1)–(4) to form the estimate of F_{px}^{melt}. In Fig. 3 we recalculate F_{px}^{melt} using a variety of trace element pairs. The important result from Fig. 3 is that the estimate of F_{px}^{melt} is mostly independent of the trace elements chosen. The mean F_{px}^{melt} calculated from all the individual determinations in Fig. 3 is within error of that from using Nb/Zr alone. Although there are fewer isotope data than trace element data for Iceland, we show in Appendix C that the same result is also obtained by mass balancing isotope endmembers with average crustal composition.

The higher F_{px}^{melt} of central Iceland is consistent with plume driven upwelling at the base of the melt region, causing excess production of small fraction melts compared with passive plate spreading. This is in contrast to basalts from north east Iceland, for which the lower F_{px}^{melt} is consistent with derivation from an enriched mantle source undergoing passive decompression melting at a spreading centre (Maclennan et al., 2001a). In the following, we proceed with the estimate of F_{px}^{melt} obtained from north east Iceland data, because (1) it was produced using more data than from the south west (4859 versus 2395 separate geochemical observables), and (2) plume driven upwelling may not be significant, unlike central Iceland.

3. Translating F_{px}^{melt} into F_{px}^{solid}

The conversion of the mass fraction of pyroxenite derived melts (F_{px}^{melt}) into the mass fraction of pyroxenite in the source (F_{px}^{solid}) requires understanding the melting behaviour of each lithology present, as there will be a non-trivial relationship between the mass fraction of material in the source and the volume of melt produced from each lithology. A full realisation of multi-lithology mantle melting is not possible given our current understanding of the composition, extraction and reaction of melts during melting, and quantitative estimates of mantle lithological heterogeneity will therefore have to be refined as our understanding of partial melting improves. Despite these limitations, it is possible to make estimates of F_{px}^{solid} subject to some simplifying assumptions about how the melting process operates. Here we investigate a method using a simple tri-lithologic melting model, the strength of which is in making the key controls and assumptions apparent.

3.1. Modelling melting

The important assumptions inherent to the melting model we use are that melting and decompression occur isentropically, that thermal equilibrium is maintained between all lithologies, and that all lithologies and their melts are chemically isolated (see discussion in Phipps Morgan, 2001). Whilst these assumptions will be false in detail, incorporating disequilibrium processes would make the model substantially more complex without helping our understanding of what controls F_{px}^{melt} and crustal thickness (tc).

The volume of melt produced by each lithology is dependent upon a wide range of parameters describing the physical state of the melting region. Below we list the key parameters and how we have dealt with them:

1. *Mantle potential temperature.* Tp is allowed to vary from 1250–1600 °C, equivalent to an excess temperature with respect to MORB mantle of −80 to +270 °C assuming a MORB mantle Tp of 1330 °C.
2. *Mantle flow field.* The higher F_{px}^{melt} calculated from central Iceland compared with that from north east or south west Iceland (Fig. 3), supported the observation that Iceland's centre is strongly affected by plume driven upwelling, whilst at the coasts flow within the melt region is from passive plate spreading alone (Ito et al., 1999; Maclennan et al., 2001a; Kokfelt et al., 2003; Koornneef et al., 2012a). Melting calculations are therefore performed integrating over a triangular melt region (White et al., 1992; Slater et al., 2001).
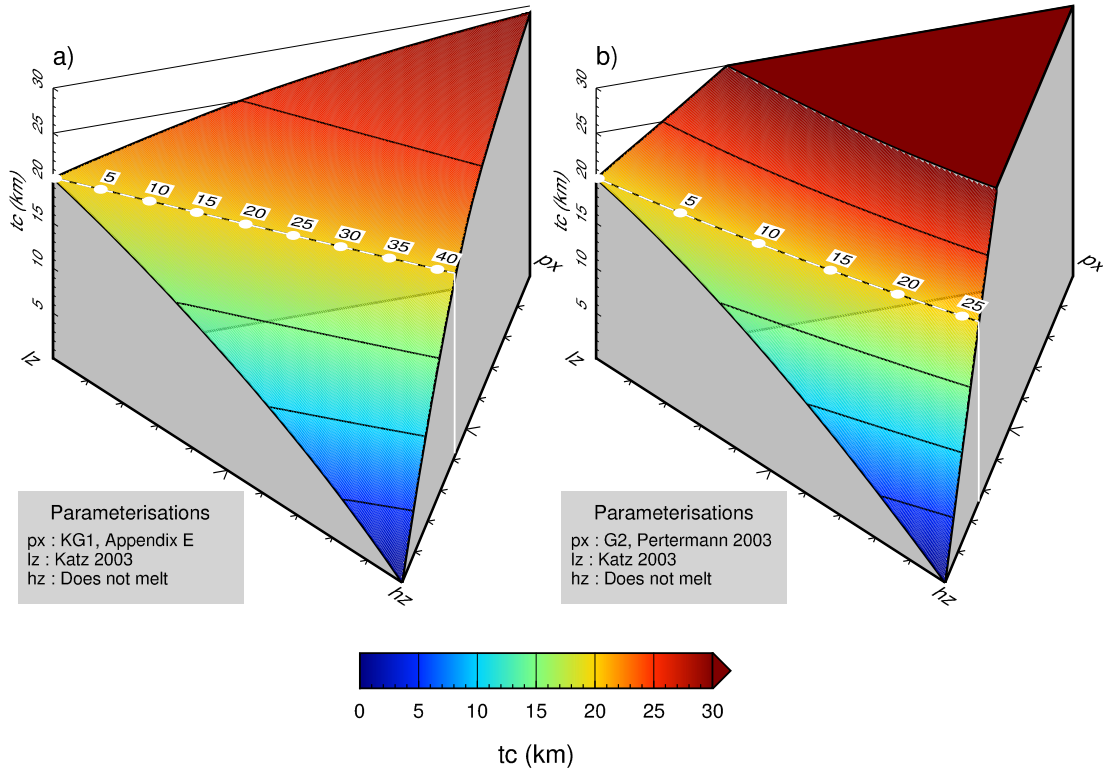
Fig. 4. 3D ternary diagrams showing the calculated crustal thickness (tc) when melting a mantle of variable lithology at Tp = 1480 °C. (a) The endmember lithologies are a lherzolite (lz, using the parameterisation for KLB-1 from Katz et al., 2003), harzburgite (hz, not modelled to melt), and pyroxenite (px, using a new parameterisation for melting the pyroxenite KG1, see Appendix D). Intermediate bulk lithologies represent a source containing a mechanical mixture of the pure endmembers. The height of the surface along the z-axis and its shading denotes the crustal thickness. The dashed white contour marks an isopleth of constant (20 km) crustal thickness, equivalent to that beneath Theistareykir and Iceland's coasts, and points along this contour are numbered by the mass fraction of pyroxenite in the lithology mixture (F_{px}^{solid}). (b) The same calculations as in (a) but now using a parameterisation for melting the more fusible G2 pyroxenite from Pertermann and Hirschmann (2003) in place of KG1. See text for details of calculations.

3. *The locations of the solidus and liquidus surfaces for each lithology.* Existing solidus and liquidus parameterisations are used for lherzolite (lz, Katz et al., 2003) and G2 pyroxenite (Pertermann and Hirschmann, 2003). We assume the harzburgite (hz) undergoes no melting, and for KG1 define a new parameterisation (see Appendix D).

4. *The productivity (dF/dP) of each lithology within the melting interval.* The parameterisations we use to define the solidus and liquidus surfaces of each lithology also provide melt fraction as a function of non-dimensionalised temperature, from which dF/dP can be calculated. In our calculations the various lithologies have productivities in the order $[dF/dP]_{G2} > [dF/dP]_{KG1} > [dF/dP]_{lz} > [dF/dP]_{hz} = 0$.

5. *The depth to the top of the melting region.* The top of the melt region is defined to be the point at which the integrated crustal pressure equals the pressure of upwelling. In this case, the thicker crust generated by having a higher Tp or more productive bulk lithology causes melting to stop deeper.

6. *Melt extraction efficiency.* We assume perfect fractional melting: instantaneous complete extraction of all melt produced.

A detailed description of the melting model can be found in Appendix D.

The following results are presented separately for a mantle containing the pyroxenite component as KG1 (a 50:50 lherzolite–basalt mixture, Kogiso et al., 1998), and the pyroxenite component as G2 (a subducted MORB, Pertermann and Hirschmann, 2003). The reason for this is that although Shorttle and Maclennan (2011) identified a homogeneous KLB-1–MORB mixture as providing the closest match to the major element composition of Icelandic melts, it is unclear whether a KG1-like source exists as a distinct lithol-

ogy prior to melting, or is generated by infiltration and reaction of melts from the basalt lithology with surrounding lherzolite. However, we show here that even with this uncertainty, the fraction of basalt in the source as inferred from using either the melting behaviour of KG1 or G2 pyroxenite is very similar.

3.2. Combining geochemical and geophysical constraints

Together, the volume of melt production and the proportion of melt from each lithology place limitations on the mantle lithology and Tp. We know from Fig. 3 that $F_{px}^{melt} = 30 \pm 10\%$, and we can add to this that crustal thickness at Iceland's coasts is ∼20 km (Staples et al., 1997; Darbyshire et al., 2000).

We first use the melting model to predict the igneous crustal thickness (tc) as a function of the source lithology mixture. The results of calculating tc are shown in Fig. 4 as a 3D ternary diagram, which along the vertical axis plots the tc generated from melting varying mechanical mixtures of lherzolite (lz), pyroxenite (px, either KG1 Fig. 4a, or G2 Fig. 4b) and harzburgite (hz) at a Tp of 1480 °C. Increasing the amount of either KG1 or G2 in the source raises the total melt production, whilst harzburgite dilutes productivity because it is not melting. Dashed white contours on each ternary mark all the lithology combinations generating a crustal thickness of 20 km, equivalent to that at Iceland's coasts. With only the crustal thickness constraint on source lithology the white contour shows that the pyroxenite fraction in the source could vary between 0 and 40%, provided the harzburgite fraction undergoes a corresponding increase to offset the pyroxenite's high productivity. Despite a range of lithology mixtures generating 20 km of crust, the key observation is that although a pure lherzolite mantle is a valid solution for matching tc alone, it would necessarily
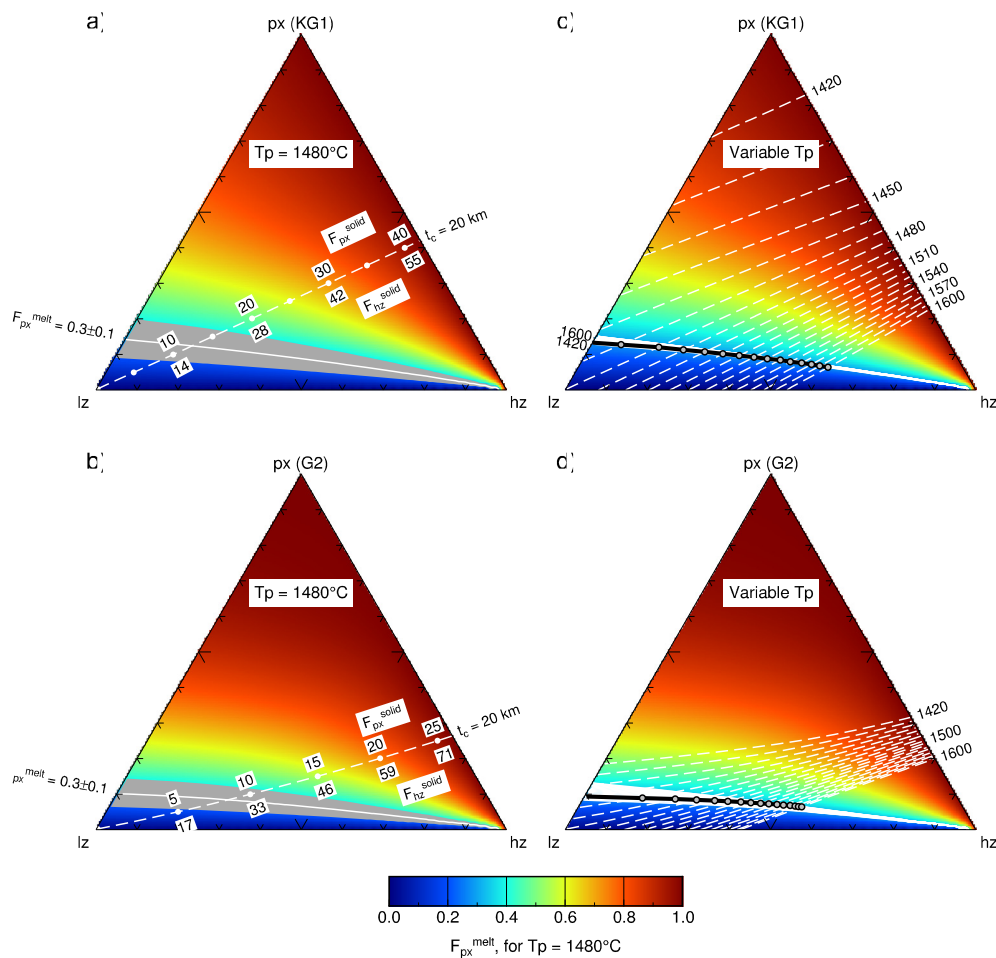
Fig. 5. Ternary diagrams combining crustal thickness (tc) and geochemical constraints (F_{px}^{melt}) to identify the allowable lithology combinations beneath Iceland. Each apex of the ternary represents an endmember lithology in the mantle: lherzolite (lz), harzburgite (hz) and pyroxenite (px, for (a) and (c) the KG1 composition from Kogiso et al., 1998, for (b) and (d) the G2 composition from Pertermann and Hirschmann, 2003). The three endmember lithologies are mechanically mixed in variable proportions and three-lithology melting calculations performed to fill in the ternary space for F_{px}^{melt} and tc. Background colours in these diagrams correspond to F_{px}^{melt} determined for model runs with Tp = 1480°C. (a) and (b) All calculations are performed at a mantle potential temperature of 1480°C. The dashed white line marks the lithology combinations melting to produce a tc = 20 km, the solid white line and grey shaded region mark the lithology combinations reproducing the observed $F_{px}^{melt} = 0.3 \pm 0.1$. The point of intersection of the solid and dashed white lines is the lithology mixture able to match both crustal thickness and geochemical constraints (in (a) this is $lz_{71}hz_{17}px_{12}$, in (b) $lz_{70}hz_{22}px_8$). (c) and (d) Melting calculations are repeated for a range of Tp to explore its effect on our ability to estimate the lithology of the source. With variable Tp a series of lithology mixtures are able to match tc and F_{px}^{melt}, these possible solutions are shown by a thick solid black line. Grey circles show the points where the solid white lines (F_{px}^{melt} constraint) and dashed lines (tc constraint) intersect for each different Tp. Only mantle potential temperatures $\geqslant$1465°C in (c), and $\geqslant$1455°C in (d), provide valid solutions.

create a crust where $F_{px}^{melt} = 0$, inconsistent with what we found in Section 2.

In Fig. 5 we have combined the requirements for the melting model to match tc and generate 30% of the crust from pyroxenite derived melts. The ternary diagrams in Figs. 5a and 5b relate source lithology to F_{px}^{melt} (coloured surface), overlaid onto which is the tc = 20 km contour (dashed white line from Fig. 4) and the $F_{px}^{melt} = 30$% contour (solid white line, with grey region marking the $\pm$10% uncertainty). The intersection of these two lines defines the lithology combination that can match both tc and F_{px}^{melt}. With KG1 as the pyroxenite component, the mantle at the point of intersection between the tc and F_{px}^{melt} contours is $lz_{71}hz_{17}px_{12}$ (Fig. 5a), whilst with G2 the intersection is at $lz_{70}hz_{22}px_8$ (Fig. 5b). Separating the KG1 lithology into its constituent basalt and lherzolite components, the mantle source found in Fig. 5a is $lz_{77}hz_{17}px_6$. So given a Tp of 1480°C, the mantle lithology beneath Iceland contains 4–10% basalt (or 8–15% KG1), 13–33% harzburgite and 83–57% lherzolite.

These estimates of source lithology are predicated upon independently knowing Tp. If Tp is not known then a family of F_{px}^{melt}–tc intersections are generated, shown in Figs. 5c and 5d as grey cir-

cles connected by a thick black line. As the Tp of the calculations increases, the tc = 20 km contour moves towards the harzburgite apex, with increased amounts of the un-melting harzburgite offsetting the extra melt generation from lherzolite and pyroxenite. In contrast, the position of the $F_{px}^{melt} = 30$% contour is not a strong function of Tp: it undergoes a slight decrease as Tp increases, but an F_{px}^{melt} between 4 and 10% is a feature of all solutions.

Figs. 5c and 5d also place a lower limit on the Tp of the Icelandic mantle. The locus of viable mantle lithologies (thick black line) intersects the lherzolite–pyroxenite join at a Tp $\sim$ 1460°C (Figs. 5c and 5d), any Tp lower than this is unable to generate the required tc without forming too much of the crust from pyroxenite derived melts.

4. Implications of lithology for plume buoyancy

Mantle plumes are a natural consequence of high Rayleigh number convection in planetary interiors. Originating at thermal boundary layers, plumes rise from depth as thermal expansion lowers their density with respect to cooler ambient mantle. Almost as soon as the plume theory had been developed (Wilson, 1963;

Table 1
Starting compositions for the three lithology endmembers used in density modelling, in mole %.

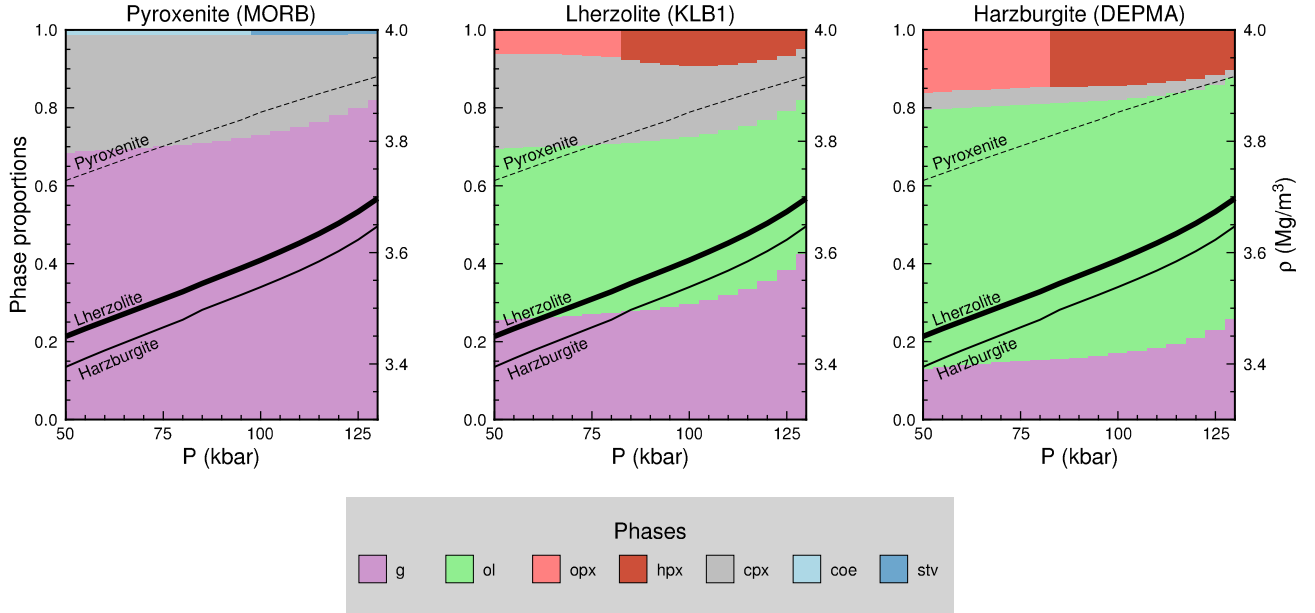| Lithology	SiO$_2$	Al$_2$O$_3$	CaO	MgO	FeO	Na$_2$O	Sum
Pyroxenite (MORB)[a]	52.15	9.90	12.75	12.30	10.10	2.80	100.00
Lherzolite (KLB-1)[b]	39.53	2.01	3.31	49.67	5.22	0.26	100.00
Harzburgite (DEPMA)[c]	36.60	0.90	1.08	55.70	5.70	0.02	100.00

[a] Kogiso et al. (1998).
[b] Hirose and Kushiro (1993).
[c] Laporte et al. (2004).

Fig. 6. Phase proportions (mole %) and densities for three bulk compositions, MORB (Kogiso et al., 1998), KLB-1 lherzolite (Hirose and Kushiro, 1993), and the DEPMA harzburgite (Laporte et al., 2004), calculated using THERMOCALC (Holland and Powell, 1998) over an upper mantle pressure range and 1300 °C adiabat. The phase proportions calculated from each bulk composition are given on the left axes and represented by coloured vertical bars, the densities are given on the right axes and represented in the plots as black lines. g = garnet, ol = olivine, opx = orthopyroxene, hpx = high pressure pyroxene, cpx = clinopyroxene, coe = coesite, and stv = stishovite. The tc-ds62 dataset used in running THERMOCALC is from Holland et al. (2013), which is a revision of that released by Holland and Powell (2011). Activity–composition relations are from Holland et al. (2013), which uses the garnet model from White et al. (2000) and the pyroxene model from Green et al. (2012).

Morgan, 1971), it became apparent that ocean islands represent not only thermal, but also compositional anomalies (Tatsumoto, 1966; Hubbard, 1969). In the previous section we demonstrated that for Iceland this compositional anomaly is likely to be due in part to the presence of recycled material, which we modelled as a basalt–harzburgite mixture. Lithological heterogeneity has a dynamical significance that trace element and isotopic heterogeneity does not: it implies sources with different major element compositions and mineralogies, which in turn will have different densities, heat capacities and thermal expansivities. Using thermodynamic modelling to estimate the densities of different sources, we now assess the dynamical implications of lithological heterogeneity.

4.1. Density of the Icelandic mantle

We use THERMOCALC (Holland and Powell, 1998) with the revised dataset tc-ds62 from Holland et al. (2013) to compute the phase assemblages and densities of endmember lherzolite, pyroxenite, and harzburgite lithologies. The bulk compositions for each lithology used in the calculations can be found in Table 1. We only consider external plume buoyancy here, i.e. that of the bulk plume material with respect to the ambient mantle (assumed to be KLB-1-type lherzolite with Tp = 1300 °C). Internal buoyancy, that of the individual heterogeneities with respect to the plume's dominant, or matrix, lithology, is neglected for the following reasons: (1) Stokes' settling velocities for even kilometer sized heterogeneities with 300 kg m^{-3} density excesses are small compared to

likely rates of plume ascent; (2) full modelling of internal plume re-organisation, especially considering a tri-lithologic mantle in which some plume lithologies could be buoyant with respect to the matrix, would require a dynamical model and is beyond the scope of this paper.

The density and mineralogy for each lithology over an upper mantle pressure range are shown in Fig. 6, for a calculation performed at a Tp = 1300 °C. The DEPMA harzburgite lithology is distinct from KLB-1 lherzolite by having greater proportions of olivine and less garnet and pyroxene, whilst a MORB composition pyroxenite is olivine free and composed almost entirely of garnet and clinopyroxene, with minor amounts of coesite or stishovite. These differences in mineralogy and composition between the three lithologies give rise to differences in density such that $\rho_{hz} < \rho_{lz} < \rho_{px}$ (Fig. 6). Given the >280 kg m^{-3} excess density of pyroxenite compared with lherzolite, it is clear that to maintain plume buoyancy with a large fraction of entrained pyroxenite will require a large excess temperature and/or a compensating low density harzburgite fraction.

In Fig. 7a we calculate the excess density of plume mantle ($\Delta\rho = \rho(\text{plume}) - \rho(\text{ambient})$, where ambient mantle is assumed to be 100% lherzolite), having a Tp = 1500 °C and at a pressure of 70 kbar. The ternary in Fig. 7 is coloured by $\Delta\rho$, where blue indicates regions where the plume mantle has positive excess density and is negatively buoyant, red indicates negative excess density and therefore positive plume buoyancy, and white is the point of neutral buoyancy. Overlaid on top of the red–white–blue $\Delta\rho$
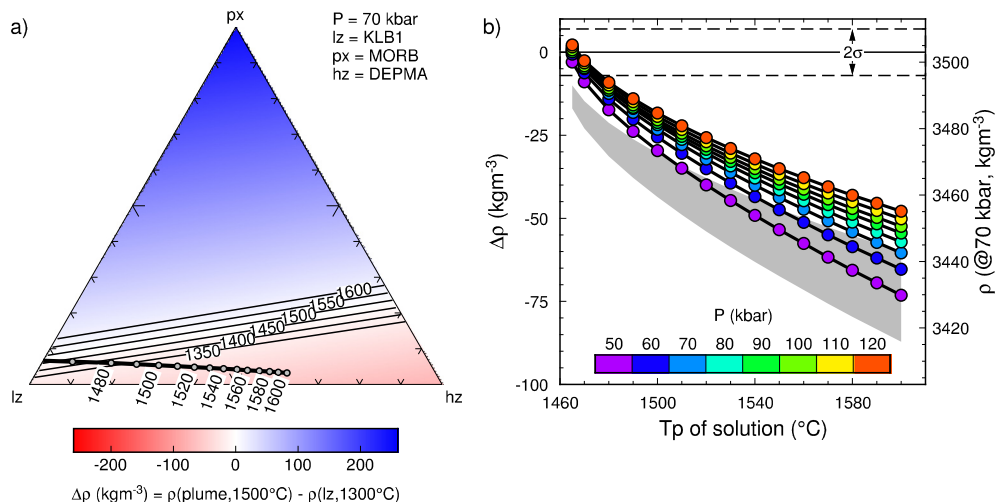
Fig. 7. The density difference ($\Delta\rho$) between lherzolite, harzburgite and pyroxenite lithology mechanical mixtures and a reference mantle column of 100% lherzolite at 1300 °C. (a) The fitting Icelandic source compositions are mapped onto a three lithology ternary diagram to determine their buoyancy in the upper mantle. As in Fig. 5, the thick solid black line represents the range of solutions for which the lithology mixtures are able to match tc and F_{px}^{melt} constraints at different mantle potential temperatures. The ternary diagram is coloured for the density excess/deficit of a 1500 °C mantle plume with respect to reference lherzolitic mantle at 70 kbar, however, the thin black lines also drawn indicate the locus of neutrally buoyant lithology mixtures for a range of plume potential temperatures: above these lines (on the high px side) lithology mixtures are negatively buoyant, whilst below they are positively buoyant. (b) $\Delta\rho$ for each lithology solution, plotted against the potential temperature of that solution. Points are coloured by the pressure at which the densities have been calculated, 50–120 kbar, representing most of the depth range of the upper mantle. Note that moving along the x-axis represents both a change in potential temperature and bulk composition of the source. The grey region marks the $\Delta\rho$ for when the plume is referenced to a mantle column containing 5% pyroxenite and 95% lherzolite. All calculations were performed using THERMOCALC (Holland and Powell, 1998). The horizontal dashed lines around 0 represent a 2σ uncertainty on the density calculations, propagated from the uncertainty on mineral endmember volumes. (For interpretation of the references to colour in this figure, the reader is referred to the web version of this article.)

surface is a thick black line joining grey circles, this marks the lithology solutions we found for Iceland, labelled by the Tp for which they are valid. For example, the 1500 °C lithology solution lies in the light red region in Fig. 7a, indicating that it is less dense than the reference KLB-1 mantle and therefore positively buoyant. Strictly, the surface in Fig. 7a is only appropriate when plume Tp = 1500 °C, i.e. for only one of the possible lithology solutions. To address this, Fig. 7b directly plots the $\Delta\rho$ for all lithology solutions over an upper mantle pressures range, using the potential temperatures for which the solutions are valid. Almost all lithology solutions for Iceland are buoyant in the upper mantle; only the Tp = 1465 °C lithology solution (a pure lherzolite–pyroxenite mixture) is close to neutral or negative buoyancy (Fig. 7b).

It is implicit in the relative density calculations performed above that we know the lithology of the ambient mantle (we assumed 100% lherzolite). However, estimates of ambient mantle lithology from Hirschmann and Stolper (1996) and Sobolev et al. (2007) have suggested that it may contain as much as 5% MORB-like pyroxenite component. If there is pyroxenite embedded in lherzolitic ambient mantle then this mixture will have a higher bulk density than the lherzolite alone and relatively increase the buoyancy of mantle plumes (assuming that there is not also a complementary harzburgite fraction in ambient mantle, which would tend to counter this effect). The significance of a 95:5 lherzolite:pyroxenite ambient mantle for our density calculations is shown by the grey field in Fig. 7b. By including 5% pyroxenite in the ambient mantle, plume buoyancy increases by ~12 kg m^{-3}. This is a small effect compared to the total positive buoyancy of the hottest and most harzburgitic Iceland plumes (~70 kg m^{-3}), but is enough that the 1465 °C solutions (lz$_{87}$hz$_0$px$_{13}$) that were neutrally buoyant when the ambient mantle was purely lherzolite, now have the same positive buoyancy as the original 1490 °C plume mantle (lz$_{66}$hz$_{23}$px$_{11}$) had with respect to lherzolite. Therefore, in terms of using merely the presence or absence of plume positive buoyancy to isolate viable plume lithologies, this uncertainty the lithology of the ambient mantle could have a large effect. In part to address this uncertainty we next consider how the

calculated plume densities translate into plume dynamics, specifically a plume's volume flux.

4.2. How a plume's lithology affects its volume flux

Plumes are driven by having a lower density than ambient mantle, so the wide range of $\Delta\rho$ exhibited by the different lithology solutions in Fig. 7 may imply significant variations in plume strength, or volume flux. Jones et al. (2014) recently estimated volume flux for the Iceland plume from the combined geochemical and geophysical evidence for the plume material affecting ridge-segments up to 1800 km away from the plume centre. Here we use a simple analytical model to relate the $\Delta\rho$ for each of our lithology solutions to a plume volume flux, and compare this estimate with that of Jones et al. (2014). The null-hypothesis in this test is that all lithology solutions are capable of generating the required volume flux. However, from Fig. 7b it is the low Tp (harzburgite poor) lithology solutions that have the lowest buoyancy, which if they struggle to match the Jones et al. (2014) volume flux constraint will imply a finite harzburgite fraction in the source and Tp > 1460 °C.

The equation to relate $\Delta\rho$ to the volume flux through a deformable plume conduit is (Turcotte and Schubert, 2002),

$$Q_v = \frac{\pi}{8} \frac{\Delta\rho\, g r^4}{\mu_p}, \tag{5}$$

where g is gravity, r is the radius of the conduit and μ_p is the viscosity of the plume (Fig. 8a). Eq. (5) is a significant simplification of plume flow, but is meaningful provided viscosity in the plume conduit is substantially less than that of ambient mantle; a condition that should be met by the temperature dependence of viscosity (Karato and Wu, 1993), and our estimated minimum plume temperature excess of 130 °C.

In Eq. (5) we use a fixed viscosity of 10^{19} Pa s and plume conduit radius of 100 km (Fig. 8b). The use of Eq. (5) with these parameter values in three ways errs on the side of supporting the null-hypothesis that all solutions will generate high volume fluxes:
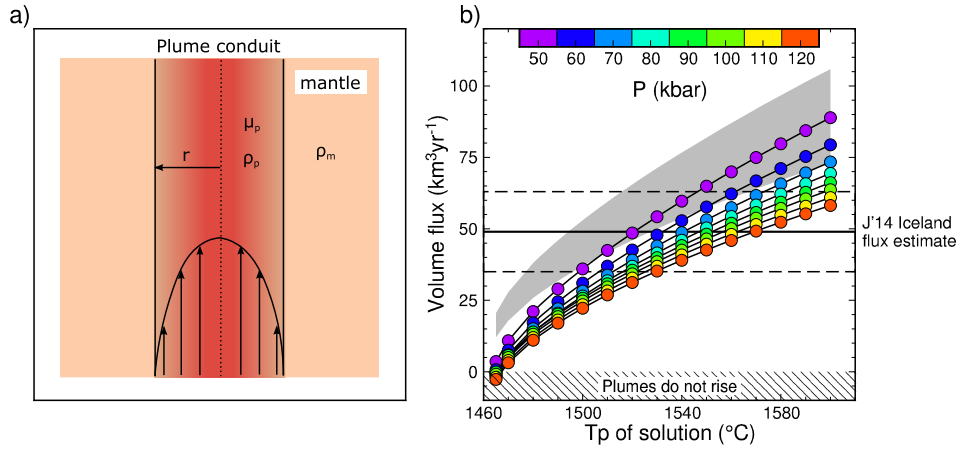
Fig. 8. Model calculations using the density contrast of the different lithology solutions for Iceland to predict the plume volume flux and compare it with the Jones et al. (2014) determination. (a) A cartoon of the model calculation where the plume tail is modelled as a cylindrical pipe (Turcotte and Schubert, 2002); r is conduit radius, μ is the viscosity, and ρ is the density, where subscript 'p' indicates plume and 'm' the mantle. (b) Model calculations solving Eq. (5) with a 100 km radius conduit and plume viscosity of 10^{19} Pa s. The density contrast between ambient mantle (100% lherzolite) and the plume is a function of pressure, so volume flux for each of the lithology solutions has been calculated at a range of pressures corresponding to most of the depth range of the upper mantle, points are coloured by the pressure used. The horizontal solid and dashed lines mark the plume flux estimate from Jones et al. (2014), $Q_v = 49 \pm 14$ km^3 yr^{-1}. The grey region indicates how the solutions shift if the ambient mantle is assumed to contain 5% pyroxenite component, this increases its density thereby making the plume more buoyant.

(1) we consider $r = 100$ km from tomographic estimates (Rickers et al., 2013), however the resolution of the tomographic models means 100 km must be an upper limit on conduit radius and consequently overestimate Q_v in Eq. (5); (2) $\mu_p = 10^{19}$ Pa s is low given that glacio-isostatic estimates of upper mantle viscosity are $\sim 10^{21}$ Pa s (Peltier, 1996), and is still reasonable even considering the approximately ten-fold decrease in viscosity per 100 °C of temperature excess (Schubert et al., 2001); (3) the form of Eq. (5) linearly relates increases in $\Delta\rho$ to Q_v, however boundary layer scalings for an isoviscous fluid imply that $Q_v \propto$ Ra$^{1/3}$ (where Ra is Rayleigh number), so in applying Eq. (5) we are likely to be overestimating the scaling of Q_v with increasing $\Delta\rho$. All these factors make our volume flux estimates conservative with regard to arguing for high plume temperatures and significant refractory components.

Using the parameters discussed above we calculate Q_v over an upper mantle pressure range (Fig. 8b). The key result of Fig. 8b is that a volume flux equal to the 49 ± 14 km^3 yr^{-1} estimate of Jones et al. (2014) is only able to be attained across the whole upper mantle pressure range by those lithology solutions with high Tp ($\geqslant 1500$ °C) and significant harzburgite fraction ($\geqslant 30\%$). The lithology solutions with Tp < 1500 °C have low predicted $\Delta\rho$ and volume fluxes due to their low F$_{hz}^{solid}$, high F$_{px}^{solid}$, and low Tp, and cannot reproduce the Jones et al. (2014) estimate of Iceland's volume flux. Importantly, this result holds even when plume buoyancy is enhanced by comparison to an ambient mantle that contains 5% pyroxenite.

In Appendix E we show that allowing our choice of parameter values to vary, conduit radii $\leqslant 120$ km and viscosities $\geqslant 0.5 \times 10^{19}$ Pa s all still require greater source buoyancy than produced by the lowest Tp-lithology solutions. Therefore, even with the uncertainty in making volume flux estimates, the conservative nature of our calculations makes it likely that to meet the volume flux estimate of Jones et al. (2014), a plume substantially hotter than the minimum Tp solution of 1465 °C is required, and thus also a source with a significant harzburgite fraction.

4.3. Buoyancy of lithology estimates in other settings

The density calculations performed above allow the buoyancy and dynamical plausibility of the suggested source lithologies from other settings to be assessed. Few quantitative estimates of source lithology exist and, as far as we are aware, no other workers have quantified lithology proportions for a lherzolite–pyroxenite–harzburgite mantle. As a result, the source estimates we overlay onto the 1450 °C and 1600 °C neutral buoyancy contours in Fig. 9a have all been plotted at constant F$_{px}^{solid}$, but over the full range of F$_{hz}^{solid}$ and F$_{lz}^{solid}$.

The important result of Fig. 9 is that the mantle lithologies identified by several authors for Hawaii (Sobolev et al., 2005; Pietruszka et al., 2013) are not buoyant as simple lherzolite–pyroxenite mixtures in the upper mantle, even with excess temperatures of 270 °C. Instead, up to 40% of the Hawaiian source must be harzburgite (or another low density lithology) for the plume to both contain $\sim 20\%$ recycled basalt and have positive buoyancy (Fig. 9b). Alternatively, the mass fraction of pyroxenite in the Hawaiian source has been overestimated, and although some volcanoes may be supplied almost exclusively by pyroxenite derived melts, the bulk source has much less pyroxenite in it. This latter possibility reminds us of the difficulty of estimating source lithology from basalt geochemistry, especially in dynamically complex regions like Hawaii, where the melting process that is so dominant a control on the manifestation of source heterogeneity is itself poorly understood.

5. Summary: a recipe for quantifying lithological heterogeneity

To make an estimate of mantle lithological heterogeneity from an initial identification of geochemical heterogeneity in erupted basalts requires multiple steps, each of which involves assumptions about processes that are themselves poorly understood. The procedure we developed here considered a three lithology lherzolite–pyroxenite–harzburgite mantle and took the following steps:

1. Identify the geochemical characteristics of endmember depleted and enriched melts.
2. Determine the composition of the aggregate melt from the melting region.
3. Calculate the fractional contribution of enriched and depleted melts to the aggregate melt by calculating a mass balance between the aggregate and endmember melt compositions.
4. Use the major element compositions of the endmember melts to isolate the mantle lithologies they correspond to Shorttle and Maclennan (2011).
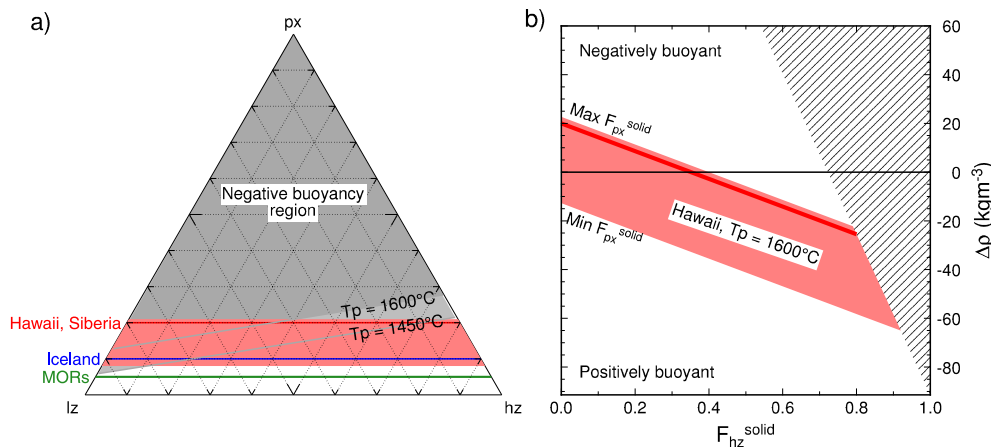
Fig. 9. The buoyancy of mantle source lithologies inferred to be feeding volcanism in a variety of settings. (a) Literature estimates of the amount of F_{lz}^{solid} and F_{px}^{solid} are overlaid onto the 1450 and 1600 °C plume–neutral buoyancy contours (solid grey lines) from Fig. 7 (assuming 100% lherzolite ambient mantle). Solid coloured lines are F_{px}^{solid} estimates from Hirschmann and Stolper (1996) and Sobolev et al. (2007, 2008), the light red region is the range of lherzolite:pyroxenite estimates for Hawaiian volcanism from Pietruszka et al. (2013). None of the literature F_{px}^{solid} values explicitly consider a harzburgite fraction in the mantle, so they have been drawn to cover the range of possible F_{hz}^{solid} given the estimated F_{px}^{solid}. It should be noted that these ranges do not preserve the lherzolite to pyroxenite ratio implicit in the authors' original estimates, other than for when $F_{hz}^{solid} = 0$. (b) The density difference between hypothesised Hawaiian plume sources and ambient mantle ($\Delta\rho$), plotted as a function of harzburgite fraction in the source; calculated with Tp = 1600 °C. (For interpretation of the references to colour in this figure legend, the reader is referred to the web version of this article.)

5. Produce a tri-lithologic melting model, containing enriched, depleted and refractory domains to predict F_{px}^{melt} and tc as a function of source lithology and Tp.
6. Combine observational constraints on F_{px}^{melt} and tc to delimit viable mantle source lithologies and Tp.

The result of these calculations indicates that the mantle under Iceland must contain 4–10% pyroxenite and have an excess potential temperature ⩾130 °C. A variation in lithology alone cannot reproduce the geophysical and geochemical observations, which require the Icelandic mantle to also have a significant temperature excess compared with typical mid-ocean ridges.

For the purposes of producing simple testable models, in this manuscript we have only considered a mantle comprising a lherzolite, pyroxenite, and harzburgite mixture. This three-lithology source represents a large reduction in mantle lithological complexity, away from of what must really be a continuum in the major element chemistry of mantle rocks. However, what is important is that the three lithologies we use are representative of the gross inputs and outputs of mantle differentiation. Therefore, our finding of a finite proportion of each of lherzolite, pyroxenite, and harzburgite lithologies in the Icelandic source is in all likelihood evidence for the continuous nature of mantle lithological variability, which ranges from both more refractory and more fertile domains.

If refractory domains are an important part of the mantle lithological spectrum, as our results suggest, this means there is a greater need to combine geochemical observations with geophysical constraints to overcome their often chemically cryptic role in mantle melting. In this manuscript we explored one additional constraint, that of the plume's volume flux and how it is affected by the range of viable source lithologies and potential temperatures of the Icelandic mantle. From the requirement to match Iceland's estimated volume flux it is likely that in addition to containing recycled pyroxenite, the Icelandic mantle contains a mass fraction of refractory component ⩾30%.

Acknowledgements

Appendix A. Identifying lithological heterogeneity: major element–trace element relationships

Shorttle and Maclennan (2011) used plots of Nb/Zr versus MgO with individual points coloured by their major element composition to relate lithological heterogeneity to enrichment. These plots allowed primitive samples to be identified that had avoided significant mixing and crystallisation, both of which can introduce erroneous correlations between major elements and indices of enrichment. The MgO range of primitive samples was ⩾9.5 wt% MgO and those samples have been plotted in Fig. A.1 directly against their major element composition. Major element–trace element trends are similar between north and south Iceland and clearly reproduce the association between high FeO, low CaO and enrichment (high Nb/Zr). These major element characteristics are inconsistent with melting of a single lherzolite lithology at a range of pressures or melt fractions, and instead require lithological variability in the source (Shorttle and Maclennan, 2011).

Appendix B. Nb/Zr as a conservative tracer

We define a conservative tracer during fractional crystallisation as one that is not fractionated by the removal of crystallising phases, so that despite a change in the concentration of elements forming the tracer during magmatic evolution, its value stays constant. The best example would be a radiogenic isotope ratio such as $^{87}Sr/^{86}Sr$, of which the equilibrium fractionation between isotopes during crystallisation is very small (and in any case corrected for during analysis), so that a single batch of magma evolving in isolation would have the same $^{87}Sr/^{86}Sr$ after 99% crystallisation as it did at 0%. However, as we discuss in Appendix C, the abundance of isotope data is less than that of trace elements so we chose to use an incompatible trace element ratio with a similar resistance to the fractionation process as an isotope ratio.

The equation describing the evolution of a trace element ratio (C_l^i/C_l^j, for elements i and j in the liquid) during fractional crystallisation is,
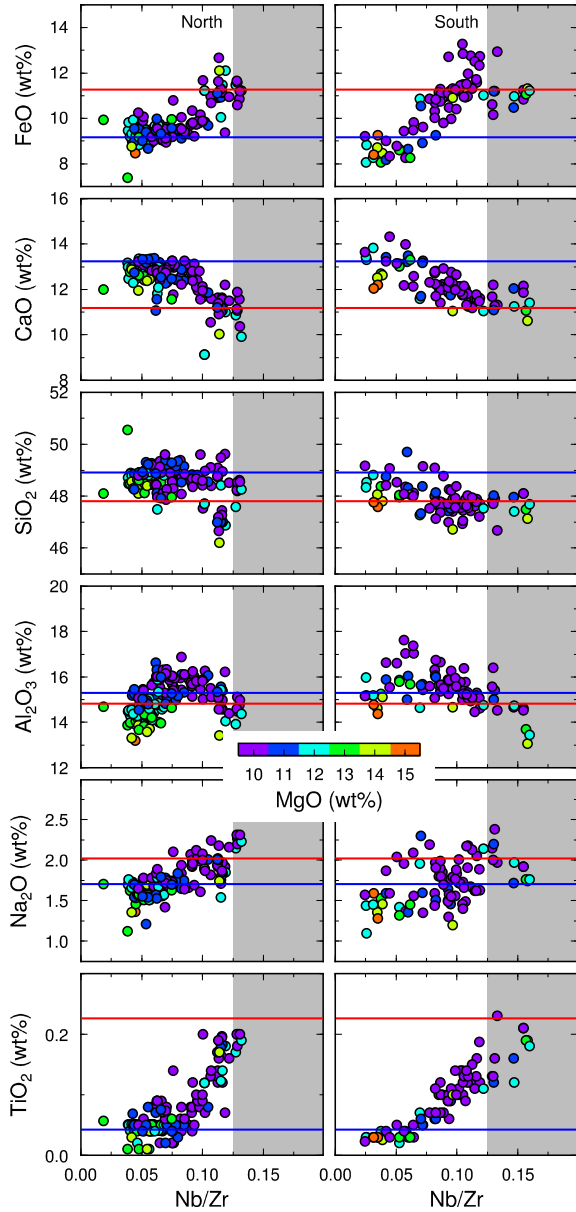
Fig. A.1. The relationship between incompatible trace element ratio Nb/Zr and major element composition of Icelandic basalts. Only basalts with MgO ⩾ 9.5 (wt%) have been plotted and points are coloured by their MgO concentration. The left panel of plots includes basalts from Iceland's centre and north, the right panel basalts from Iceland's southwest. Red and blue horizontal lines mark the enriched and depleted Icelandic melt composition respectively, identified by Shorttle and Maclennan (2011). (For interpretation of the references to colour in this figure legend, the reader is referred to the web version of this article.)

$$\frac{C_l^i}{C_l^j} = \frac{C_0^i}{C_0^j} F^{(D_i - D_j)}, \tag{B.1}$$

where F is the degree of crystallisation. Eq. (B.1) shows that the minimum offset of the final trace element ratio from the original (C_0^i / C_0^j), is when the difference in partition coefficients between the two elements $(D_i - D_j)$ is close to zero. In general this condition is met for any pair of D_i and D_j that are similar, but will also hold when both elements are highly incompatible $(D \ll 1)$, in which case even order of magnitude differences in D_i and D_j will give $|D_i - D_j| \ll 1$.

To demonstrate the systematics of crystallisation and mixing in the crust, we used Nb/Zr ratios (Fig. 1). We reproduce the first panel from Fig. 1 here, overlaid with a model calculation of how
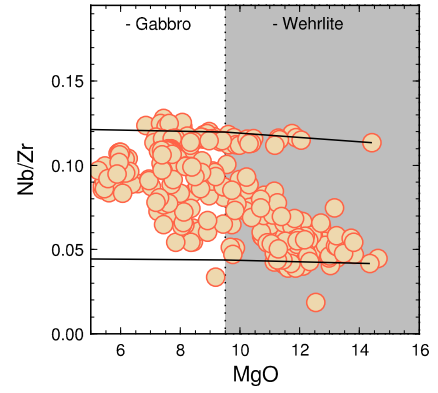

Fig. B.2. Whole-rock Nb/Zr from Theistareykir and Krafla basalts overlaid with black lines modelling how the Nb/Zr of primitive basalts is predicted to evolve during fractional crystallisation alone. The relationship between the degree of crystallisation and MgO was taken from Maclennan et al. (2001b), with 20% of the starting mass lost to wehrlite ($ol_{69}cpx_{30}plag_1$) removal between 14 and 9.5 wt% MgO, followed by gabbro ($ol_7cpx_{40}plag_{53}$) removal to 5 wt% MgO, by which point 80% of the starting system mass has been lost to crystallisation.

fractional crystallisation alone would affect the Nb/Zr of primitive melts (Fig. B.2, details of calculation in caption). Fig. B.2 shows that Nb/Zr ratios are minimally affected by fractional crystallisation, even though 80% of the starting system mass is lost during evolution from ∼14 to 5 wt% MgO (Maclennan et al., 2001b).

We subsequently expanded our analysis from looking at Nb/Zr alone, to using a range of trace elements (Fig. 3). To demonstrate that this selection of trace elements and their ratios is robust to fractional crystallisation processes we have plotted matrices of $|D_i - D_j|$ for separate mineral phases (Fig. B.3) and for the bulk wehrlitic or gabbroic cumulates (Fig. B.4). The values of $|D_i - D_j|$ are greatest for clinopyroxene (Fig. B.3), but for the abundance of crystallising phases to be consistent with the major element evolution of Icelandic basalts (Maclennan et al., 2001b), almost all trace element ratios will have a $|D_i - D_j| \leqslant 0.1$ (Fig. B.4).

The small values of $|D_i - D_j|$ in the matrices of Fig. B.4 justify our use of Nb/Zr and other incompatible trace element ratios as conservative tracers during crystallisation. Our use of conservative trace element ratios means that the estimate of mean crustal composition (R_{ij} in Eq. (4)) can be reliably made, without crystal fractionation introducing a significant systematic bias to the final determination of F_{px}^{melt}.

Appendix C. Mass balance of pyroxenite and lherzolite derived melts with isotopes

Despite the arguments for incompatible trace element ratios being an appropriate proxy for source composition (Fig. 2a and Section 2.2), and their being conservative during magmatic differentiation (Appendix B), it would still be preferable to use isotope data to form the diagrams in Fig. 1 and to make the estimates of F_{px}^{melt}. The drawback of using isotopes is that there is much less data available, which means the effect of concurrent mixing and crystallisation on geochemical variability is harder to resolve. Despite this limitation, in Fig. C.5 we use Sr isotopes in place of Nb/Zr to track geochemical variability, estimate average crustal and end-member compositions, and calculate F_{px}^{melt}. The key result is that the F_{px}^{melt} estimates from Fig. C.5 using isotopic data are within uncertainty of those presented in Figs. 1 and 3 using trace element data.

Appendix D. Modelling tri-lithology mantle melting

Before developing a melting model it is necessary to identify the lithologies present in the mantle and their melting behaviour.
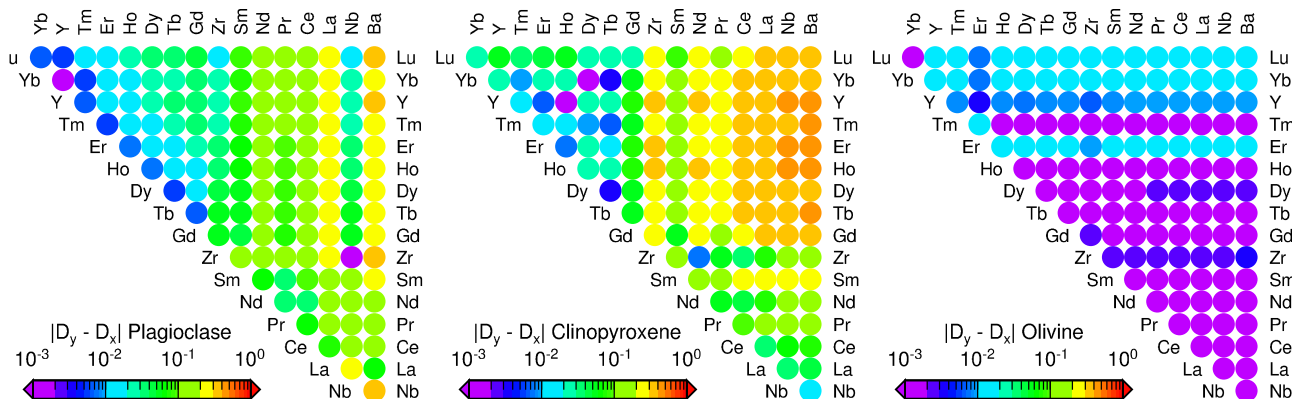
Fig. B.3. Matrices show the absolute partition coefficient difference for individual mineral phases ($|D_y - D_x|$). Elements along the top axis form the denominator partition coefficient (D_x), elements along the vertical axis the numerator partition coefficient (D_y). Partition coefficients from McKenzie and O'Nions (1991), Gibson and Geist (2010).
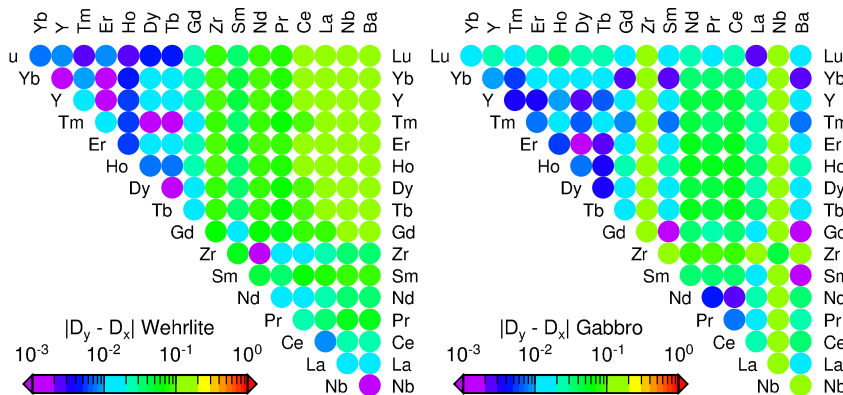

Fig. B.4. The absolute difference in bulk partition coefficients if olivine, plagioclase and clinopyroxene are crystallising in wehrlitic the proportions ($ol_{69}plag_1cpx_{30}$) or gabbroic ($ol_7plag_{53}cpx_{40}$) proportions.
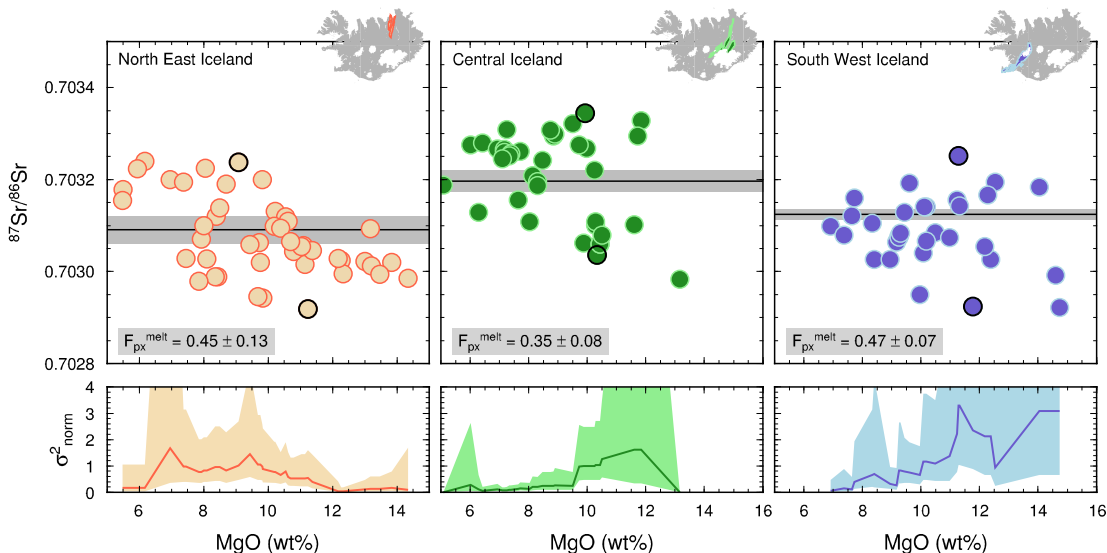

Fig. C.5. The evolution of isotopic variability and composition during concurrent crystallisation and mixing (equivalent to the trace element patterns in Fig. 1). Samples used in defining the endmember compositions are circled in black. Solid horizontal black lines marks the volume average $^{87}Sr/^{86}Sr$ with the 1 s.e. region in grey. The reason for the low estimates of uncertainty on the values of F_{px}^{melt} here compared with those in Fig. 1, is that in selecting only one sample to define an isotopic endmember we are reducing the apparent uncertainty in the endmember compositions, which when we used the (much more abundant) trace element data was obtained by calculating the standard deviation of the highest and lowest 10% of samples.

There is abundant geochemical evidence for at least one enriched and one depleted source in the Icelandic mantle, corresponding to pyroxenite and lherzolite lithologies respectively (Shorttle and Maclennan, 2011). In this paper we consider the melting of a lherzolite and pyroxenite lithology (two types of the latter), as well as

allowing for variable amounts of harzburgite to be present. Refractory lithologies in the mantle may be difficult to detect geochemically; they would contribute little if any melt to the total melt production, and any melts produced would have low concentrations of the incompatible trace elements (Sr, Nd, Pb) whose isotope
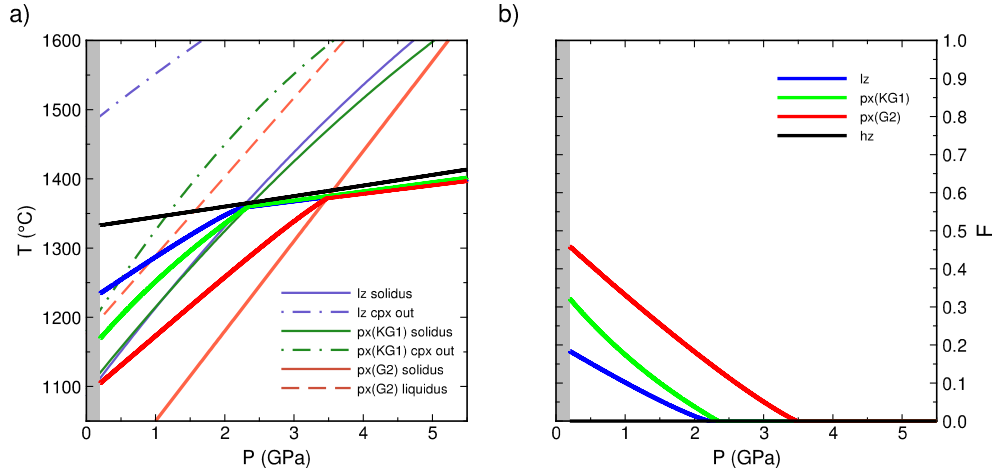
Fig. D.6. Results of model calculations melting single lithology mantles of lherzolite (lz), pyroxenite (G2 or KG1, Pertermann and Hirschmann, 2003; Kogiso et al., 1998) or harzburgite (hz) at a mantle potential temperature of 1330 °C. (a) Pressure–temperature paths for a column of single lithology mantle undergoing isentropic decompression, followed by melting once it has intersected its solidus. Mantle P–T paths are indicated by thick solid lines, solidus, liquidus and clinopyroxene out (cpx out) boundaries for each lithology are marked by thin solid or dashed lines. Because the harzburgite is constrained to undergo no melting it defines a simple adiabat (Eq. (D.3)) for the whole pressure range. The shaded area marks the crustal thickness applied in these calculations, and therefore the pressure at which the melting calculations stop. (b) The degree of melting for a packet of mantle undergoing the maximum amount of decompression.

systems are most frequently used to characterise source. However, there is evidence from Hf isotopes that highly refractory domains exist and are sampled by melting in some locations (Salters et al., 2011). Given also that we are envisaging a recycled origin for the pyroxenite component it seems inevitable that the complementary depleted lithologies would be recycled as well, and so may form a significant, albeit cryptic, fraction of any mantle source containing recycled material.

At least three equations are needed to parameterise the melting of a lithology, (1) an equation for the location of the solidus surface in temperature–pressure space, $T_s(P)$, (2) an equation for the liquidus surface, $T_l(P)$, and (3) an equation describing how the melt fraction varies across the melting interval, $F(P, T')$, where T' is the dimensionless scaled temperature $T' = (T - T_s)/(T_l - T_s)$. Further, each of these expressions needs to be differentiable: dT_l/dP, dT_s/dP, $[dT/dF]_P$, $[dT/dP]_F$.

For lherzolite melting we use the parameterisation of Katz et al. (2003), which splits melting up into a higher productivity clinopyroxene–present melting interval, followed by a low productivity clinopyroxene absent melting interval. The refractory harzburgite we assume never undergoes melting. This is a simplifying assumption, but is probably appropriate in the case when the harzburgite is a minority component in the source, in which case heat loss from the harzburgite to the other melting lithologies will keep the harzburgite chilled below its solidus. We model the melting of two pyroxenitic lithologies. The G2 lithology from Pertermann and Hirschmann (2003) is a MORB-like composition, with the result that it is an extreme case of a low solidus temperature and high productivity (narrow melting interval). We also create a parameterisation for the KG1 composition, which like the lherzolite lithology of Katz et al. (2003) we break into a cpx present melting interval described by a solidus surface,

$$T_s = -4.7P^2 + 124.1P + 1095.4, \tag{D.1}$$

and clinopyroxene out surface,

$$T_{cpx\text{-}out} = -11.1P^2 + 157.2P + 1179.6. \tag{D.2}$$

To parameterise the solidus and cpx-out surfaces and the isobaric melt production of KG1, we used a method similar to that used by Pertermann and Hirschmann (2003) for the pyroxenite G2 and Lambart et al. (2013) on the pyroxenite MIX1G, assuming that F is

a quadratic function of temperature (T) up to the cpx-out. Following clinopyroxene out we then use the liquidus surface for harzburgite from Katz et al. (2003), which creates a low productivity tail to KG1 melting. The relevant solidus, liquidus and clinopyroxene out surfaces for each lithology are shown in Fig. D.6, along with the simplest case of single lithology melting for each source lithology.

The basic parameters describing the melting process are the productivity dF/dP and the temperature evolution of the (solid) source dT/dP. These terms are derived by Phipps Morgan (2001) by forming an entropy balance assuming isentropic melting (i.e. reversible and adiabatic) for an n-lithology mantle. We reproduce the key results below for the three lithology mantle we consider.

The adiabat for a three lithology mantle, in the absence of melting, is given by,

$$T = T_0 \exp\left(\frac{\sum^{n=3} \phi_n \frac{\alpha_n}{\rho_n}}{\sum^{n=3} \phi_n Cp_n} P\right) \tag{D.3}$$

where T_0 is the mantle potential temperature, P – the pressure, Cp – the heat capacity, ϕ_n – the mass fraction of a given lithology n such that $\sum^n \phi_n = 1$, α – the thermal expansivity and ρ is the density.

In most cases (all cases we model in this paper), within an ascending parcel of a lithologically heterogeneous mantle, the fusible pyroxenite lithology (KG1 or G2) will intersect its solidus first. In this case, heat from the lherzolite and harzburgite flows to the pyroxenite as it consumes heat undergoing the transition from a low entropy solid to high entropy liquid. The equation for temperature evolution during perfect fractional melting in this interval is,

$$\frac{dT}{dP} = \frac{dF}{dP}\left[\frac{dT}{dF}\right]_P^{px} + \left[\frac{dT}{dP}\right]_F^{px}, \tag{D.4}$$

and the productivity of the pyroxenite is given by,

$$\frac{dF}{dP} = -\frac{\frac{\overline{Cp}}{T}\left[\frac{dT}{dP}\right]_F^{px} - (\overline{\alpha/\rho})}{\phi_{px}\Delta S_f^{px} + \frac{\overline{Cp}}{T}\left[\frac{dT}{dF}\right]_P^{px}}, \tag{D.5}$$

where ϕ is the mass fraction of each lithology in the source, ΔS_f is the entropy of fusion, $\overline{Cp} = \phi_{px}Cp_{px} + \phi_{pd}Cp_{pd} + \phi_{hz}Cp_{hz}$, and $(\overline{\alpha/\rho}) = \phi_{px}\frac{\alpha_{px}}{\rho_{px}} + \phi_{pd}\frac{\alpha_{pd}}{\rho_{pd}} + \phi_{hz}\frac{\alpha_{hz}}{\rho_{hz}}$.

The next stage of melting is for the lherzolite to intersect its solidus, then potentially both pyroxenite and lherzolite lithologies

Table D.1
Parameters used in the melting calculations.

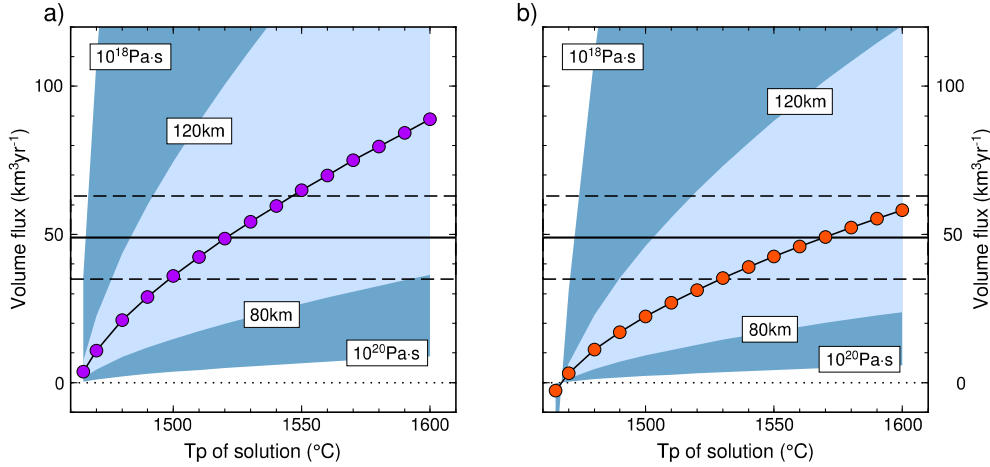| Parameter	Lherzolite	Pyroxenite		Harzburgite	Units
		KG1	G2		
Mass fraction cpx	0.15[a]	–	–	–	
Heat capacity	1187	1140	1140	1000	J kg^{-1} K^{-1}
Thermal expansivity, solid	30×10^{-6}	30×10^{-6}	30×10^{-6}	30×10^{-6}	K^{-1}
Density, solid	3300	3300	3550	3250	kg m^{-3}
Density, liquid	2900	2900	2900	2900	kg m^{-3}
Entropy of fusion	407	380	380	–	J kg^{-1} K^{-1}

[a] Required for the lherzolite parameterisation of Katz et al. (2003).

Fig. E.7. Model calculations to assess the sensitivity of the plume volume flux estimates to the chosen conduit radius and plume viscosity. In each figure the connected coloured circles are the volume flux estimates for the Icelandic lithology solutions as shown in Fig. 8b, and the solid and dashed lines mark the volume flux estimate of 49 ± 14 km^3 yr^{-1} from Jones et al. (2014). (a) Illustrates how the volume flux estimate for the density contrast at 50 kbar varies as a function of the conduit radius (light blue region, 80 km–120 km) and plume viscosity (dark blue region, 10^{18} Pa s–10^{20} Pa s). (b) Variation in the plume flux estimate for the 120 kbar density contrast. (For interpretation of the references to colour in this figure legend, the reader is referred to the web version of this article.)

will be melting depending upon their relative $[dT/dP]_F$. In the dual lithology melting case, dT/dP is again given by Eq. (D.4) (because thermal equilibrium has to be maintained between all lithologies), but the dF/dP used is the bulk productivity, which in the absence of harzburgite melting is given by,

$$\frac{dF}{dP} = \phi_{px}\left[\frac{dF}{dP}\right]^{px} + \phi_{pd}\left[\frac{dF}{dP}\right]^{pd}. \tag{D.6}$$

The individual productivities in this case are,

$$\left[\frac{dF}{dP}\right]^{px} = -\frac{\frac{\overline{Cp}}{T}\left[\frac{dT}{dP}\right]^{px}_F - (\overline{\alpha/\rho}) + \phi_{pd}\Delta S^{pd}_f \frac{\left(\left[\frac{dT}{dP}\right]^{px}_F - \left[\frac{dT}{dP}\right]^{pd}_F\right)}{[dT/dF]^{pd}_P}}{\phi_{px}\Delta S^{px}_f + \phi_{pd}\Delta S^{pd}_f \frac{[dT/dF]^{px}_P}{[dT/dF]^{pd}_P} + \frac{\overline{Cp}}{T}\left[\frac{dT}{dF}\right]^{px}_P}, \tag{D.7}$$

and for lherzolite,

$$\left[\frac{dF}{dP}\right]^{pd} = \frac{[dT/dF]^{px}_P}{[dT/dF]^{pd}_P}\left[\frac{dF}{dP}\right]^{px} + \frac{\left[\frac{dT}{dP}\right]^{px}_F - \left[\frac{dT}{d}\right]^{pd}_F}{\left[\frac{dT}{dF}\right]^{pd}_p}. \tag{D.8}$$

Parameters for these calculations can be found in Table D.1. The differential equations describing melting are numerically integrated using a fourth-order Runge–Kutta scheme (Press et al., 1992). Integration to calculate total pressure of the crust is performed using,

$$P_c = \int \frac{F}{1-F}\,dP, \tag{D.9}$$

which accounts for compaction of the melting region in response to melt extraction (Eq. (6) of White et al., 1992). Integration begins at the onset of melting and stops when $P_c \geqslant P$, i.e. when the

mantle column has upwelled to the base of the crust. Conversion between P_c and tc, the crustal thickness, is made by assuming the crust has a mean density of 2900 kg m^{-3} (Menke, 1999).

Because the harzburgite is modelled to never undergo melting, Eqs. (D.4)–(D.8) are very similar to the two lithology melting equations from Phipps Morgan (2001). The main difference is that the harzburgite heat capacity term appears in the numerator and denominator of Eqs. (D.6) and (D.5) for dF/dP, the effect of which is to thermally buffer the melting of lherzolite and pyroxenite lithologies.

Appendix E. Varying viscosity and conduit radius in plume flux calculations

Neither plume viscosity (μ_p) nor plume conduit radius (r) are independently and exactly known. A maximum plume conduit radius can be estimated from seismic tomographic images, and a lower bound on viscosity can be placed by considering estimates of upper mantle viscosity and the likely scaling of viscosity with temperature. These considerations led us in Section 4.2 to use a viscosity of 10^{19} Pa s and conduit radius of 100 km. These parameters indicated that the low Tp-lithology solutions for Iceland could not generate sufficiently high plume volume flux Jones et al. (2014). Here we test the sensitivity of that result to variations in r and μ_p.

Panels a and b of Fig. E.7 explore how varying the plume conduit radius between 80 and 120 km and viscosity by two orders of magnitude affects the predicted volume flux. Conduit radii up to 120 km still require Tp-lithology solutions with Tp $> 1480\,°$C and $>15\%$ harzburgite fraction in the source, whilst if the conduit is narrower than 100 km both the Tp and harzburgite fraction must

substantially increase to maintain the volume flux. Viscosity has a strong control over volume flux because of the potential magnitude of its variation within the Earth. Any $\mu_p > 0.5 \times 10^{19}$ Pa s requires finite harzburgite fraction, but if μ_p is as low as 10^{18} Pa s, then the Tp-lithology solutions with the lowest $\Delta\rho$ are capable of generating the Iceland plume's volume flux, but only in the shallowest upper mantle (Fig. E.7a).

An accurate relation of buoyancy to plume volume flux is highly model and parameter dependent. However, within reasonable bounds, the low Tp-lithology solutions are unable to generate the volume flux seen at Iceland.

Appendix F. Data sources

Here we list the sources of geochemical data used in Figs. 1, 2 and 3. For north east Iceland data were taken from: Skovgaard et al. (2001), Breddam et al. (2000), Maclennan et al. (2001b, 2001a, 2003), Slater et al. (2001), Stracke et al. (2003), Nicholson et al. (1991), Kokfelt et al. (2006), Koornneef et al. (2012b). For central Iceland data were taken from: Hémond et al. (1993), Chauvel and Hémond (2000), Maclennan et al. (2001a), Shorttle et al. (2013), Kokfelt et al. (2006), Breddam (2002), Hardarson and Fitton (1997). For south west Iceland data were taken from: Skovgaard et al. (2001), Hémond et al. (1993), Chauvel and Hémond (2000), Sinton et al. (2005), Eason and Sinton (2009), Kokfelt et al. (2006), Koornneef et al. (2012b), Hardarson and Fitton (1997), Gee et al. (1998a, 1998b), Thirlwall et al. (2004), Peate et al. (2009).

References

Allègre, C.J., Turcotte, D.L., 1986. Implications of a two-component marble-cake mantle. Nature 323, 123–127.

Breddam, K., 2002. Kistufell: primitive melt from the Iceland mantle plume. J. Petrol. 43, 345–373.

Breddam, K., Kurz, M.D., Storey, M., 2000. Mapping out the conduit of the Iceland mantle plume with helium isotopes. Earth Planet. Sci. Lett. 176, 45–55.

Chase, C.G., 1981. Oceanic island Pb: two-stage histories and mantle evolution. Earth Planet. Sci. Lett. 52, 277–284.

Chauvel, C., Hémond, C., 2000. Melting of a complete section of recycled oceanic crust: trace element and Pb isotopic evidence from Iceland. Geochem. Geophys. Geosyst. 1.

Darbyshire, F.A., White, R.S., Priestley, K.F., 2000. Structure of the crust and uppermost mantle of Iceland from a combined seismic and gravity study. Earth Planet. Sci. Lett. 181, 409–428.

Eason, D.E., Sinton, J.M., 2009. Lava shields and fissure eruptions of the Western Volcanic Zone, Iceland: Evidence for magma chambers and crustal interaction. J. Volcanol. Geotherm. Res. 186, 331–348.

Fitton, G.J., Saunders, A.D., Norry, M.J., Hardarson, B.S., Taylor, R.N., 1997. Thermal and chemical structure of the Iceland plume. Earth Planet. Sci. Lett. 153, 197–208.

Fitton, G.J., Saunders, A.D., Kempton, P.D., Hardarson, B.S., 2003. Does depleted mantle form an intrinsic part of the Iceland plume?. Geochem. Geophys. Geosyst. 4.

Gee, M.A.M., Taylor, R.N., Thirlwall, M.F., Murton, B.J., 1998a. Glacioisostacy controls the chemical and isotopic characteristics of tholeiites from Reykjanes Peninsula, SW Iceland. Earth Planet. Sci. Lett. 164, 1–5.

Gee, M.A.M., Thirlwall, M.F., Taylor, R.N., Lowry, D., Murton, B.J., 1998b. Crustal processes: major controls on Reykjanes peninsula lava chemistry, SW Iceland. J. Petrol. 39, 819–839.

Gibson, S.A., Geist, D., 2010. Geochemical and geophysical estimates of lithospheric thickness variation beneath Galápagos. Earth Planet. Sci. Lett. 300, 275–286.

Green, E.C.R., Holland, T.J.B., Powell, R., White, R.W., 2012. Garnet and spinel lherzolite assemblages in $MgO–Al_2O_3–SiO_2$ and $CaO–MgO–Al_2O_3–SiO_2$: thermodynamic models and an experimental conflict. J. Metamorph. Geol. 30, 561–577.

Hardarson, B.S., Fitton, J.G., 1997. Mechanisms of crustal accretion in Iceland. Geology 25, 1043–1046.

Hémond, C., Arndt, N., Litchenstein, U., Hofmann, A., Oskarsson, N., Steinthorsson, S., 1993. The heterogeneous Iceland plume: Nd–Sr–O isotopes and trace element constraints. J. Geophys. Res. 98, 15833–15850.

Hirose, K., Kushiro, I., 1993. Partial melting of dry peridotites at high pressures: determination of compositions of melts segregated from peridotite using aggregates of diamond. Earth Planet. Sci. Lett. 114, 477–489.

Hirschmann, M.M., Stolper, E.M., 1996. A possible role for garnet pyroxenite in the origin of the "garnet signature" in MORB. Contrib. Mineral. Petrol. 124, 185–208.

Hofmann, A.W., 1997. Mantle geochemistry: the message from oceanic volcanism. Nature 385, 219–229.

Hofmann, A.W., White, W.M., 1982. Mantle plumes from ancient oceanic crust. Earth Planet. Sci. Lett. 57, 421–436.

Holland, T.J.B., Powell, R., 1998. An internally consistent thermodynamic dataset for phases of petrological interest. J. Metamorph. Geol. 16, 309–343.

Holland, T.J.B., Powell, R., 2011. An improved and extended internally consistent thermodynamic dataset for phases of petrological interest, involving a new equation of state for solids. J. Metamorph. Geol. 29, 333–383.

Holland, T.J.B., Hudson, N.F.C., Powell, R., Harte, B., 2013. New thermodynamic models and calculated phase equilibria in NCFMAS for basic and ultrabasic compositions through the transition zone into the uppermost lower mantle. J. Petrol. 54, 1901–1920.

Hubbard, N.J., 1969. A chemical comparison of oceanic ridge, Hawaiian tholeiitic and Hawaiian alkalic basalts. Earth Planet. Sci. Lett. 5, 346–352.

Ito, G., Shen, Y., Hirth, G., Wolfe, C.J., 1999. Mantle flow, melting, and dehydration of the Iceland mantle plume. Earth Planet. Sci. Lett. 165, 81–96.

Jones, S.M., Murton, B.J., Fitton, J.G., White, N.J., Maclennan, J., Walters, R.L., 2014. A joint geochemical–geophysical record of time-dependent mantle convection south of Iceland. Earth Planet. Sci. Lett. 386, 86–97.

Karato, S., Wu, P., 1993. Rheology of the upper mantle: a synthesis. Science 260, 771–778.

Katz, R.F., Spiegelman, M., Langmuir, C.H., 2003. A new parametrization of hydrous mantle melting. Geochem. Geophys. Geosyst. 4.

Kempton, P.D., Fitton, J.G., Saunders, A.D., Nowell, G.M., Taylor, R.N., Hardarson, B.S., Pearson, G., 2000. The Iceland plume in space and time: a Sr–Nd–Pb–Hf study of the North Atlantic rifted margin. Earth Planet. Sci. Lett. 177, 255–271.

Kerr, A.C., Saunders, A.D., Tarney, J., Berry, N.H., Hards, V.L., 1995. Depleted mantle-plume geochemical signatures: no paradox for plume theories. Geology 23, 843–846.

Kogiso, T., Hirose, K., Takahashi, E., 1998. Melting experiments on homogeneous mixtures of peridotite and basalt: application to the genesis of ocean island basalts. Earth Planet. Sci. Lett. 162, 45–61.

Kokfelt, T.F., Hoernle, K., Hauff, F., 2003. Upwelling and melting of the Iceland plume from radial variation of $^{238}U–^{230}Th$ disequilibria in postglacial volcanic rocks. Earth Planet. Sci. Lett. 214, 167–186.

Kokfelt, T., Hoernle, K., Hauff, F., Fiebig, J., Werner, R., Garbe-Schönberg, D., 2006. Combined trace element and Pb–Nd–Sr isotope evidence for recycled oceanic crust (upper and lower) in the Iceland mantle plume. J. Petrol. 47, 1705–1749.

Koornneef, J.M., Stracke, A., Bourdon, B., Grönvold, K., 2012a. The influence of source heterogeneity on the U–Th–Pa–Ra disequilibria in post-glacial tholeiites from Iceland. Geochim. Cosmochim. Acta 87, 243–266.

Koornneef, J.M., Stracke, A., Bourdon, B., Meier, M.A., Jochum, K.P., Stoll, B., Grönvold, K., 2012b. Melting of a two-component source beneath Iceland. J. Petrol. 53, 127–157.

Lambart, S., Laporte, D., Schiano, P., 2009. An experimental study of pyroxenite partial melts at 1 and 1.5 GPa: implications for the major-element composition of mid-ocean ridge basalts. Earth Planet. Sci. Lett. 282, 335–347.

Lambart, S., Laporte, D., Schiano, P., 2013. Markers of the pyroxenite contribution in the major-element compositions of oceanic basalts: review of the experimental constraints. Lithos 160–161, 14–36.

Laporte, D., Toplis, M.J., Seyler, M., Devidal, J.L., 2004. A new experimental technique for extracting liquids from peridotite at very low degrees of melting: application to partial melting of depleted peridotite. Contrib. Mineral. Petrol. 146, 463–484.

Maclennan, J., 2008a. Concurrent mixing and cooling of melts under Iceland. J. Petrol. 49, 1931–1953.

Maclennan, J., 2008b. Lead isotope variability in olivine-hosted melt inclusions from Iceland. Geochim. Cosmochim. Acta 72, 4159–4176.

Maclennan, J., McKenzie, D., Grönvold, K., 2001a. Plume-driven upwelling under central Iceland. Earth Planet. Sci. Lett. 194, 67–82.

Maclennan, J., McKenzie, D., Grönvold, K., Slater, L., 2001b. Crustal accretion under northern Iceland. Earth Planet. Sci. Lett. 191, 295–310.

Maclennan, J., McKenzie, D., Hilton, F., Gronvöld, K., Shimizu, N., 2003. Geochemical variability in a single flow from northern Iceland. J. Geophys. Res. 108.

McKenzie, D., O'Nions, R.K., 1991. Partial melt distributions from inversion of rare earth element concentrations. J. Petrol. 32, 1021–1091.

Menke, W., 1999. Crustal isostasy indicates anomalous densities beneath Iceland. Geophys. Res. Lett. 26, 1215–1218.

Morgan, W.J., 1971. Convection plumes in the lower mantle. Nature 230, 42–43.

Nicholson, H., Condomines, M., Fitton, J.G., Fallick, A.E., Gronvöld, K., Rogers, G., 1991. Geochemical and isotopic evidence for crustal assimilation beneath Krafla, Iceland. J. Petrol. 32, 1005–1020.

Peate, D.W., Baker, J.A., Jakobsson, S.P., Waight, T.E., Kent, A.J.R., Grassineau, N.V., Skovgaard, A.C., 2009. Historic magmatism on the Reykjanes Peninsula, Iceland: a snap-shot of melt generation at a ridge segment. Contrib. Mineral. Petrol. 157, 359–382.

Peltier, R., 1996. Mantle viscosity and ice-age ice sheet topography. Science 273, 1359–1364.

Pertermann, M., Hirschmann, M.M., 2003. Partial melting experiments on a MORB-like pyroxenite between 2 and 3 GPa: constraints on the presence of pyroxenite in the basalt source regions from solidus location and melting rate. J. Geophys. Res. 108.

Phipps Morgan, J., 2001. Thermodynamics of pressure release melting of a veined plum pudding mantle. Geochem. Geophys. Geosyst. 2. http://dx.doi.org/10.1029/2000GC000049.

Pietruszka, A.J., Norman, M.D., Garcia, M.O., Marske, J.P., Burns, D.H., 2013. Chemical heterogeneity in the Hawaiian mantle plume from the alteration and dehydration of altered oceanic crust. Earth Planet. Sci. Lett. 361, 298–309.

Press, W.H., Teukolsky, S.A., Vetterling, W.T., Flannery, B.P., 1992. Numerical Recipes in Fortran, second edition. Cambridge University Press.

Prinzhofer, A., Lewin, E., Allègre, C.J., 1989. Stochastic melting of the mantle: evidence from local study of the East Pacific Rise at 12°50′N. Earth Planet. Sci. Lett. 92, 189–206.

Rickers, F., Fitchner, A., Trampert, J., 2013. The Iceland–Jan Mayen plume system and its impact on mantle dynamics in the North Atlantic region: evidence from full-waveform inversion. Earth Planet. Sci. Lett. 367, 39–51.

Ringwood, A.E., 1962. A model for the upper mantle. J. Geophys. Res. 67, 857–867.

Rudge, J.F., Maclennan, J., Stracke, A., 2013. The geochemical consequences of mixing melts from a heterogeneous mantle. Geochim. Cosmochim. Acta 114, 112–143.

Salters, V.J.M., Mallick, S., Hart, S.R., Langmuir, C.E., Stracke, A., 2011. Domains of depleted mantle: new evidence from hafnium and neodymium isotopes. Geochem. Geophys. Geosyst. 12.

Schubert, G., Turcotte, D.L., Olson, P., 2001. Mantle Convection in the Earth and Planets. Cambridge University Press.

Shorttle, O., Maclennan, J., 2011. Compositional trends of Icelandic basalts: implications for short-lengthscale lithological heterogeneity in mantle plumes. Geochem. Geophys. Geosyst. 12.

Shorttle, O., Maclennan, J., Piotrowski, A.M., 2013. Geochemical provincialism in the Iceland plume. Geochim. Cosmochim. Acta 122, 363–397.

Sinton, J., Grönvold, K., Sæmundsson, K., 2005. Postglacial eruptive history of the Western Volcanic Zone, Iceland. Geochem. Geophys. Geosyst. 6.

Skovgaard, A.C., Storey, M., Baker, J., Blusztajn, J., Hart, S.R., 2001. Osmium–oxygen isotopic evidence for a recycled and strongly depleted component in the Iceland mantle plume. Earth Planet. Sci. Lett. 194, 259–275.

Slater, L., McKenzie, D., Gronvöld, K., Shimizu, N., 2001. Melt generation and movement beneath Theistareykir, NE Iceland. J. Petrol. 42, 321–354.

Sobolev, A.V., Hofmann, A.W., Sobolev, S.V., Nikogosian, I.K., 2005. An olivine-free mantle source of Hawaiian shield basalts. Nature 434, 412–417.

Sobolev, A.V., Hofmann, A.W., Kuzmin, D.V., Yaxley, G., Arndt, N.T., Chung, S.L., Danyushevsky, L.V., Elliott, T., Frey, F.A., Garcia, M.O., Gurenko, A.A., Kamenetsky, V.S., Kerr, A.C., Krivolutskaya, N.A., Matvienkov, V.V., Nikogosian, I.K., Rocholl, A., Sigurdsson, I.A., Sushchevskaya, N.M., Teklay, M., 2007. The amount of recycled crust in sources of mantle derived melts. Science 316, 590–597.

Sobolev, A.V., Hofmann, A.W., Brügmann, G., Batanova, V.G., Kuzmin, D.V., 2008. A quantitative link between recycling and osmium isotopes. Science 321, 321.

Staples, R.K., White, R.S., Brandsdóttir, B., Menke, W., Maguire, P.K.H., McBride, J.H., 1997. Färoe–Iceland Ridge experiment 1. Crustal structure of northeastern Iceland. J. Geophys. Res. 102, 7849–7866.

Stracke, A., Salters, V.J.M., Sims, K.W.W., 1999. Assessing the presence of garnet-pyroxenite in the mantle sources of basalts through combined hafnium–neodymium–thorium isotope systematics. Geochem. Geophys. Geosyst. 1.

Stracke, A., Zindler, A., Salters, V.J.M., McKenzie, D., Blichert-Toft, J., Albarède, F., Grönvold, K., 2003. Theistareykir revisited. Geochem. Geophys. Geosyst. 4.

Stracke, A., Snow, J.E., Hellebrand, E., von der Handt, A., Bourdon, B., Birbaum, K., Gunther, D., 2011. Abyssal peridotite Hf isotopes identify extreme mantle depletion. Earth Planet. Sci. Lett. 208, 359–368.

Tatsumoto, M., 1966. Genetic relations of oceanic basalts as indicated by lead isotopes. Science 153, 1094–1101.

Thirlwall, M.F., 1995. Generation of Pb isotopic characteristics of the Iceland plume. J. Geol. Soc. (Lond.) 152, 991–996.

Thirlwall, M.F., Gee, M.A.M., Taylor, R.N., Murton, B.J., 2004. Mantle components in Iceland and adjacent ridges investigated using double-spike Pb isotope ratios. Geochim. Cosmochim. Acta 68, 361–386.

Turcotte, D.L., Schubert, G., 2002. Geodynamics, second edition. Cambridge University Press.

White, R.S., McKenzie, D., O'Nions, K., 1992. Oceanic crustal thickness from seismic measurements and rare earth element inversions. J. Geophys. Res. 97, 19683–19715.

White, R.W., Powell, R., Holland, T.J.B., Worley, B., 2000. The effect of TiO_2 and Fe_2O_3 on metapelitic assemblages at greenschist and amphibolite facies conditions: mineral equilibria calculations in the system K_2O–FeO–MgO–Al_2O_3–SiO_2–H_2O–TiO_2–Fe_2O_3. J. Metamorph. Geol. 18, 497–511.

Wilson, J.T., 1963. Evidence from islands on the spreading of ocean floors. Nature 197, 536–538.